Geomorphology and evolution of the Blanes Canyon (NW Mediterranean). New insights from high resolution mapping of vertical cliffs

C. Cabrera [a,*], P. Puig [a], R. Durán [a], M-C. Fabri [b], C. Guerin [c], C. Lo Iacono [a], V.A.I. Huvenne [d]

[a] Institut de Ciències del Mar, Consejo Superior de Investigaciones Científicas (ICM-CSIC), Barcelona, Spain
[b] Institut français de recherche pour l'exploitation de la mer (Ifremer), Centre de Méditerranée, La Seyne sur Mer, France
[c] Institut français de recherche pour l'exploitation de la mer (Ifremer), Centre de Bretagne, Plouzané, France
[d] Ocean BioGeosciences, National `anography Centre, Southampton, UK

ABSTRACT

The geomorphology of the Blanes submarine canyon has been characterized based on the analysis of high-resolution hull-mounted multibeam bathymetry (up to 5 m grid size). Additionally, the Hybrid Remotely Operated Vehicle (H-ROV) *Ariane* was used to map with unprecedented detail (80 cm grid size) the morphology of vertical rockwalls on the canyon flanks, and the ROV *Liropus* was used to acquire high-resolution video footage on the same walls. The Blanes Canyon exposes well stratified Miocene and Plio-Quaternary successions dipping towards a SW direction, which are affected by NE-SW and NW-SE oriented fault systems that played an important role in the canyon development. Its structural character is evidenced by the rectilinear trajectories and sharp bends of the canyon axis and rims, the alignment of pockmark fields and the presence of vertical rockwalls. The canyon transversal profile is markedly asymmetric due to the underlying stratigraphy. The eastern flank, corresponding to the cataclinal slope characterized by strata beds dipping in the same direction as the slope, is smooth and mainly dominated by slides and toe gullies. The western flank, corresponding to the anaclinal slope facing opposite to the dip of the strata, is steeper and dominated by a dendritic network of rim gullies. H-ROV bathymetric maps and video footage of vertical walls display a wide variety of fine-scale morphological elements that evidence ongoing mass wasting and gully development as the main mechanisms involved in canyon wall retrogression. The multi-scale study of the Blanes Canyon has allowed a better characterization of the erosive processes involved in the broadening of submarine canyons and retrogression of the walls, thus contributing to the better understanding of the evolution of submarine canyons developed in tectonically controlled stratigraphic bedded sequences.

1. Introduction

Submarine canyons are deep, steep valleys incised in continental slopes and shelves all over the world (Harris and Whiteway, 2011), with the capacity to efficiently transport sediment, organic matter, and pollutants from the coast to the abyssal plain (Paull et al., 2006; Palanques et al., 2009; Zúñiga et al., 2009; Puig et al., 2014; Fisher et al., 2021). They also host and serve as habitat for numerous species that benefit from their geological substrate, hydrodynamic characteristics, and nutrient supply (Orejas et al., 2009; Fernandez-Arcaya et al., 2017; Pearman et al., 2023). Submarine canyons are sensitive to erosional and depositional processes that reshape them, conferring a complex morphological heterogeneity that is reflected at all spatial scales (Baztan

et al., 2005; He et al., 2013; Chaytor et al., 2016). The most important factors controlling the morphological characteristics and evolution of submarine canyons include: the structural and stratigraphic framework into which the canyon is incised (Shepard, 1981; Micallef et al., 2012; Bernhardt et al., 2015; Li et al., 2021); the eustatic fluctuations (Harris and Whiteway, 2011); the sedimentary inputs (Bührig et al., 2022); the oceanographic and hydrodynamic regimes (Laberg et al., 2007; Zhu et al., 2010; Durán et al., 2013; Allin et al., 2018) and, to a lesser extent, the anthropogenic impacts (Puig et al., 2012; Paradis et al., 2017).

The type of continental margin on which a submarine canyon is located largely conditions its characteristics and formation processes (Emery, 1980; Uchupi and Emery, 1991; Harris and Whiteway, 2011). In passive margins lacking active tectonic, the primary shaping processes

are related to sediment transport and deposition (Harris and Whiteway, 2011), whereas submarine canyons on margins with active tectonic, either extensional or compressional contexts, may exhibit a stronger influence of tectonic processes, such as uplift or subduction, faulting or seismic activity (Palma et al., 2021; Naranjo-Vesga et al., 2022; Mercier et al., 2023; Cerrillo-Escoriza et al., 2024). Passive margins lacking tectonic activity can also have pre-existing fault systems or weak zones inherited from earlier tectonic events that can serve as preferential pathways for erosional processes, allowing submarine canyons to develop along them and to be modified by submarine erosion (Lastras et al., 2009).

The stratigraphic architecture is also a key control on processes in submarine canyons that develop in bedded sequences, since it is a determinant factor in slope failure processes (Micallef et al., 2012). Previous observations in canyons on land have differentiated three types of slopes depending on the dipping of the strata bedding: cataclinal, orthoclinal, or anaclinal slopes (Grelle et al., 2011; Lo and Weng, 2017). Cataclinal slopes are characterized by strata dipping in the same direction as the slope face. In contrast, anaclinal slopes occur opposite to the dip of the strata, while orthoclinal slopes are defined by the azimuth of the strata dip direction orthogonal to the azimuth of the slope direction. However, the importance of slope-bedding configuration in erosive processes and the resulting morphology created during the evolution of submarine canyons has historically been overlooked.

In the last two decades, technological advances in hull-mounted multibeam systems have made it possible to operate at higher frequencies, increasing bathymetric resolutions (< 5 m pixel size) even in deeper areas (Mountjoy et al., 2009; Bernhardt et al., 2015), revealing the detailed complex morphology that characterizes submarine canyons at the mesoscale. Furthermore, the recent use of unmanned robotic vehicles, such as remotely operated vehicles (ROVs) or autonomous underwater vehicles (AUVs) has significantly enhanced the spatial resolution of seafloor mapping techniques, reaching a sub-metrical scale of seafloor complexity (Huvenne et al., 2011; Robert et al., 2017; Fabri et al., 2022). ROVs and AUVs also have the advantage of supporting video or photographic imaging systems, revealing details that remain unnoticed in the bathymetric maps, providing information on fine-scale processes occurring in the submarine canyons, such as block falls, slide scarps or active mass-wasting processes (Masson et al., 2011; Paull et al., 2013).

The use of robotic technologies is crucial for the exploration of vertical walls inside submarine canyons, as they can provide full coverage even on steep seabed slopes that remain uncovered in bathymetric data obtained from hull-mounted systems. By adjusting the multibeam echo sounder closer to the seafloor with the appropriate beam' orientation, vertical walls can be fully covered, allowing their morphological characterization, even in overhanging areas (Huvenne et al., 2011; Robert et al., 2017). There are very few fine-scale studies in the scientific literature focusing on morphological features and associated processes in submarine canyon vertical rockwalls using ROV imagery. McHugh et al. (1993) focused on the role of diagenesis and physical properties in submarine canyon with nearly vertical walls and their effect on fracture pattern and resulting morphology in the Lindenkohl, Carteret and Hendrickson canyons, offshore New Jersey (U.S. Atlantic continental margin), using ROV imagery. On the same margin, Chaytor et al. (2016) used outcrop scale ROV images to assess the different processes involved in the stability of vertical canyon rockwalls in the Oceanographer, Hudson, and Norfolk canyons. Similarly, Carter et al. (2018) used high-definition ROV imagery to study the fine-scale processes associated with rockwalls in the Whittard Canyon, on the Celtic margin.

In this paper, we characterize the broad- and fine-scale morphology of the Blanes submarine canyon (northwestern Mediterranean Sea) in unprecedented detail. At a broad-scale, this paper provides a comprehensive characterization of the canyon morphology, from the canyon head to the middle canyon, using hull-mounted high-resolution bathymetric data obtained from several oceanographic cruises. At finer scale,

the paper provides the first detailed mapping (80 cm grid size) of vertical walls within the canyon using a front-mounted ROV multibeam echosounder, in combination with High-Definition video images. The aim of this paper is to assess the dominant processes and factors involved in the shaping of submarine canyons, and particularly the role that such processes play in the development and retrogression of vertical walls within the canyon.

2. Geological setting

The Blanes Canyon is the longest (184 km) indented canyon on the Catalan margin and constitutes the southern boundary of the North Catalan Margin, in the northwestern Mediterranean (Fig. 1A) (Amblas et al., 2006; Lastras et al., 2011). The Blanes Canyon head is located at only 4 km from the coastline. The upper course exhibits an almost N-S orientation, turning in a NW-SE direction down canyon, where it eventually coalesces with the Valencia Through (Amblas et al., 2006). The Blanes Canyon divides the continental shelf in two sections, the Planassa Shelf to the northeast and the Barcelona Shelf to the southwest (Fig. 1A). The Planassa Shelf shows a dominantly rough rocky floor related to Miocene outcrops punctuated by coastal and middle shelf local accumulations of sediment (Fig. 1B; ITGE, 1989; Durán et al., 2013). The Barcelona shelf is characterized by a shallow (30 m depth) east-west sand step of 20 m high partially covered by relict prodelta deposits of the Tordera River (Lastras et al., 2011) and, unlike the Planassa, it has a depositional character supported by the presence of several large sand bodies located on the middle-outer shelf, although there is a lack of modern sediments overlying them (Durán et al., 2013, 2014).

The Blanes Canyon incises sedimentary sequences from Miocene to Plio-Quaternary ages mainly dipping in SW direction (Fig. 1B) (ITGE, 1989; Lastras et al., 2011). Three lithostratigraphic units are identified within the Miocene: the Alcanar Group, of Aquitanian and Burdigalian age, and the Castellón Group, which includes the Castellón Marls (Serravaliense - Tortonian) and Castellón Sandstones (Tortonian - Messinian) formations (ITGE, 1989). The Alcanar Group consists mainly of clays and marls, often with dolomitic characteristics, with frequent intercalations of dolomitic calcareous levels and fine sandstones. Occasionally polygenic breccias and conglomerates may occur. The Castellón Marls are composed of gray calcareous clays, with intercalations of dark siltstones and sandstones of fine to medium grain size, with quartz grains and calcareous cement. The Castellón sandstones are formed by gray silty clays somewhat calcareous, with abundant intercalations of polygenic sands and variable grain size, sometimes with calcareous cement. In the Miocene closest to the Blanes Canyon, to the west, the thickness reaches approximately 750 m, and the Alcanar Group may be missing, while to the east of the canyon, the thicknesses are lower, between 425 and 150 m, and the Middle-Upper Miocene may be missing in some areas. The Pliocene is composed of the Ebro Group, which consists of two units: the Ebro Clays (Upper Messinian - Lower Pliocene) and the Ebro Sands (Upper Pliocene or Quaternary) (ITGE, 1989). The Ebro Clays are mainly composed of marls and clays, while the Ebro Sands consist of coastal sandy and bioclastic facies. The Pleistocene corresponds lithologically to the Ebro Sands. The thickness of the Plio-Quaternary is variable, with greater thicknesses filling the Blanes subsidiary paleocanyon. The Plio-Quaternary thickness increases towards the basin, reaching thicknesses of up to 1000 m on the slope.

The Catalan margin was subjected to the occurrence of two consecutive tectonic episodes, a compressive episode after the Late Cretaceous-middle Oligocene Pyrenean, followed by a main extensive episode during Late Oligocene-early Miocene (Roca et al., 1999). These events gave rise to the rift system consisting of a NE-SW orientation horst and graben faulting (Fig. 1B) (Maillard and Mauffret, 1999; Roca et al., 1999). The post-rift stage occurred from the Early Miocene to the present and involves a series of remarkable and interrelated tectonic and depositional events, which gradually ceased during Pliocene (Roca
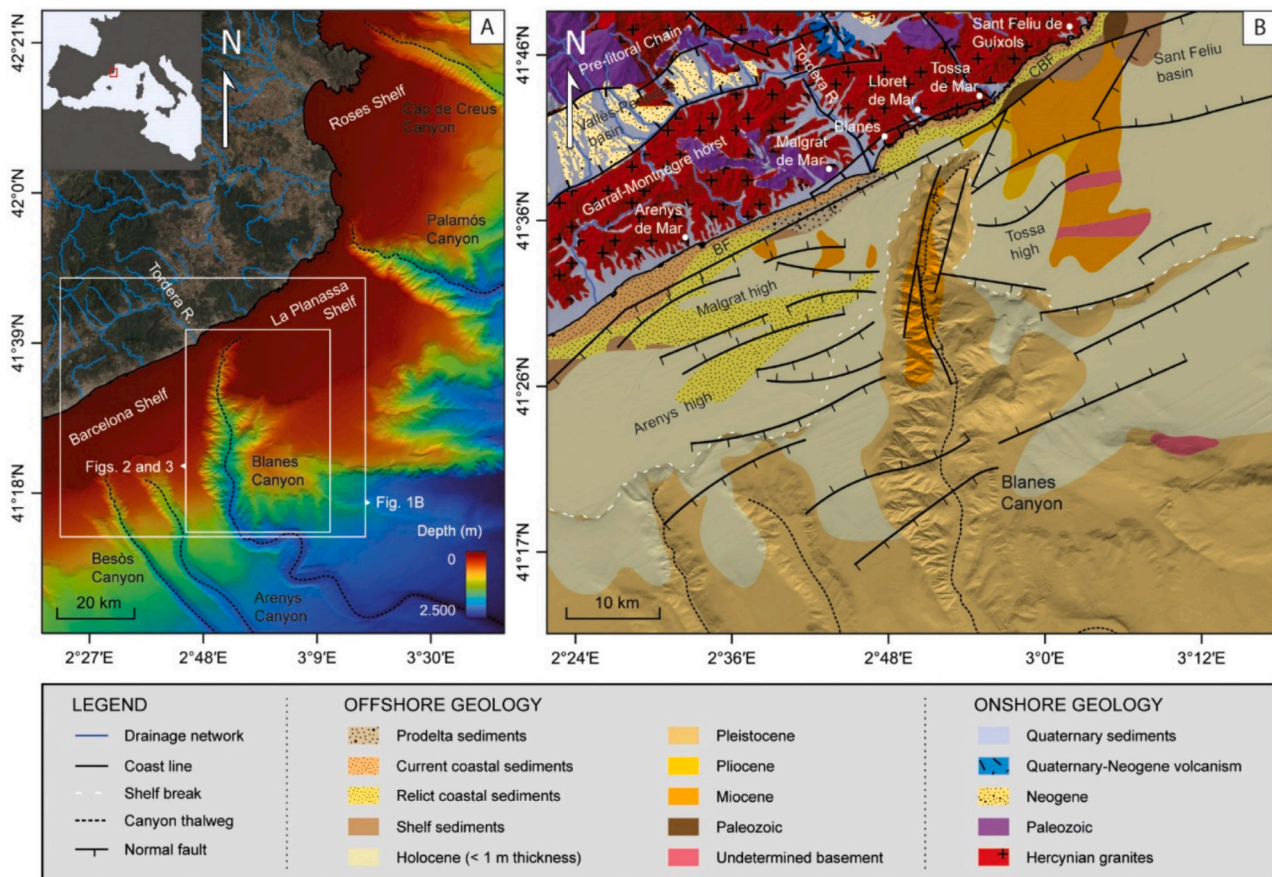
Fig. 1. (A) Location of the Blanes Canyon on the North Catalan Margin (NW Mediterranean Sea). (B) Offshore geological map of the Blanes Canyon and surrounding area. Simplified onshore geology and the fault systems that define the configuration of the area are shown. Onshore geology adapted from IGC-ICC (2010) and offshore from ITGE (1989). BF: Barcelona Fault, CBF: Costa Brava Fault.

et al., 1999). Such cessation was accompanied by an increase in the accommodation space due to the combination of the action of thermal and load subsidence due to the deposition of thick sedimentary sequences and the eustasy (Clavell and Berastegui, 1991; Amblas et al., 2006). Thermal subsidence was also related with a late extensional stage (Middle Miocene-Quaternary) during which a NW-SE fault system was reactivated as a normal faults system (Fig. 1B). During this post-rift stage, the dramatic sea level fall related to the Messinian salinity crisis led to the formation of numerous submarine canyons in the Mediterranean (Harris and Whiteway, 2011), including the submarine canyons of the northern Catalan margin (Fig. 1A) (Tassone et al., 1994; Maillard et al., 2006). Subsequently, after the reopening of the Gibraltar Strait, a series of eustatic fluctuations occurred and were recognized by the presence of major discontinuities in the Plio-Quaternary architecture linked to transgressive and regressive movements of the coastline (Serra Raventós, 1975). These shifts in coastal position have played a significant role in the feeding and re-excavation of the northern Catalan margin submarine canyons, ultimately shaping their present configuration (Maillard et al., 1992; Tassone et al., 1994). The last excavation of the Blanes Canyon took place during the Quaternary period, defining the Plio-Quaternary boundary (Serra Raventós, 1975).

3. Methodology

3.1. Data acquisition

The shallowest sector of the Blanes Canyon, from the canyon head at 52 m down to 1650 m water depth, was mapped at high resolution (5–10 m grid size) during the ABRIC-3 cruise in April–May 2021, using a hull-mounted Kongsberg-EM710 on board R/V *Ramón Margalef* (Fig. 2). The Kongsberg-EM710 uses frequencies of 70 to 100 kHz. The narrow beam forming (0.5° by 1°) and flexible frequency operation reduce the average vertical error to <0.1 % of the water depth. The high ping rate and number of beams (800 beams per ping) create a dense point cloud of soundings. The motion reference unit MRU 5+ from Kongsberg provided real-time vessel attitude values.

Multibeam bathymetry data were complemented with available datasets obtained in the preceding cruises of ABRIC project. The data from previous projects (ESPACE, HERMIONE, and ABIDES) were used to extend the covered area in the ABRIC-3 cruise and fill any gaps, with resolutions ranging between 5 and 20 m (Fig. 2). Additionally, bathymetry data from the EMODNET Bathymetry portal (90 m grid size) were used to provide background coverage for sectors lacking high resolution bathymetry. Table 1 summarizes the compilation of the bathymetries used, showing the covered area in each cruise and information related to the year of acquisition, method, multibeam echosounder system (MBES), and grid resolution.

Additionally, very high-resolution bathymetry data were gathered during the ABRIC-1 cruise in February–March 2020 on board R/V *Sarmiento de Gamboa*, using an EM2040 Kongsberg MBES operating at 300 kHz and mounted on the front of the Ifremer (French Research Institute for Exploitation of the Sea) Hybrid Remotely Operated Vehicle (H-ROV) *Ariane* (red areas in Fig. 2). The navigation system and propulsion architecture of the H-ROV *Ariane* are specially designed to work in morphologically complex canyon environments, with accurate positioning. The MBES was mounted with a 45° angle and the H-ROV transects were conducted with a constant distance of ~40 m from the wall, from deep towards shallower depths, along the walls of the canyon.
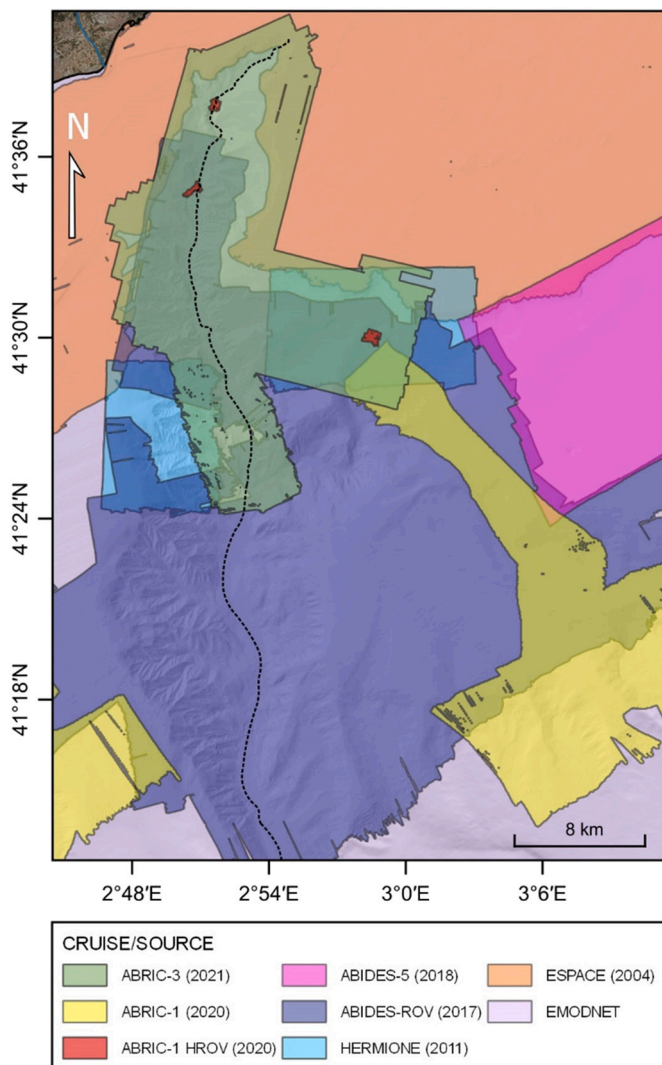
Fig. 2. Multibeam data areas used in the bathymetric compilation of the study area linked to their relative cruise and project or another source.

Table 1
Cruises/sources of the bathymetric datasets used in this study.

Cruise/Source	Date	Method	Echo sounder	Grid resolution	Area
ABRIC-3	2021	Hull-mounted	Kongsberg EM710	5 m	Canyon head and upper canyon
ABRIC-1	2020	Hull-mounted	Atlas Hydrosweep DS	20 m	Canyon and slope
ABRIC-1 HROV	2020	ROV-mounted	Kongsberg EM2040	80 cm	Vertical Walls
ABIDES-5	2018	Hull-mounted	Elac Seabeam 1050D	20 m	Upper slope
ABIDES-ROV	2017	Hull-mounted	Atlas Hydrosweep DS	20 m	Upper and middle canyon
HERMIONE	2011	Hull-mounted	Elac Seabeam 1050D	20 m	Upper canyon
ESPACE	2004	Hull-mounted	Kongsberg EM3000D	5 m	Shelf
EMODNET	–	Hull-mounted	–	90 m	Middle canyon and slope

High-definition video footage of these same canyon walls was acquired using the ROV *Liropus 2000* provided by the Spanish Institute of Oceanography (IEO) along the same transects as with the *Ariane*. The high-precision HiPAP 350P Simrad USBL acoustic system linked to the Differential Global Positioning System (DGPS) of the vessel guaranteed the underwater positioning. High-quality images were acquired using two cameras, one high definition (Kongsberg OE14–366) and one low luminosity (Kongsberg OE14–502), and one illumination system of three headlights (LED Matrix 3R Sealite) of 32 LEDs and 1700 lm in water. Four additional cameras monitored the underwater piloting operation. Liropus ROV images were used to supplement the very high-resolution bathymetric data from *Ariane*, showing its real appearance, and to visualize the smaller morphologic features under study. The images were scaled using the pair of 532 nm parallel lasers, spaced 10 cm apart.

3.2. Data processing and analysis

Post-processing of bathymetry datasets from hull-mounted echosounders was accomplished using the CARIS HIPS and SIPS 11.8 Hydrographic Data Processing System, including correction for heading, pitch, roll and heave. Tidal and sound velocity corrections were applied, and the sounding data were cleaned to remove erroneous soundings. The filtered soundings obtained for each dataset were gridded into 5 m grid digital elevation models (DEMs) for the canyon head and part of the upper canyon (i.e., ABRIC-3 cruise), and into 20 m grid DEMs for the rest of the upper and middle canyon, since resolutions vary depending on the source of the bathymetric data and the area of interest (Table 1). Slope maps, representing the slope gradient measured in degrees, were derived from the DEMs and calculated in QGIS. Backscatter data collected during ABRIC-3 cruise were processed at 5 m grid size only in the surveyed canyon head region. Post-processing of bathymetry data collected with *Ariane* was conducted using the GLOBE software, ©Ifremer (Global Oceanographic Bathymetry Explorer) (Poncelet et al., 2020). Filtered soundings were gridded into 80 cm DEMs for the three surveyed regions (Fig. 2), from which a slope map was also obtained. Backscatter data of these regions were processed at the same resolution (80 cm).

Bathymetric and backscatter datasets were projected to Universal Transverse Mercator (UTM) projection, zone 31 N, in the World Geodesic System (WGS) 1984 geographic coordinate system, and subsequently integrated into a geographic information system (QGIS and Global Mapper) for further analysis and for mapping. The backscatter strength, typically quantified in decibels (dB), is influenced by various environmental and system variables, as well as diverse seabed characteristics. These include topography (slope), micro-topography, heterogeneity within the near-surface sediments, biotic elements, and sediment properties such as grain size and sorting (Collier and Brown, 2005). Its relationship with grain size is intricate (Gaida et al., 2019); nonetheless, earlier studies have identified a positive correlation in seabed areas exhibiting consistent relief and slope variations (Goff et al., 2005; Collier and Brown, 2005). In this work, backscatter imagery was employed to qualitatively deduce seafloor slope changes, sediment texture and roughness. High reflectivity can be correlated with steep slopes and rocky outcrops, whereas low reflectivity corresponds to gentle seafloor areas. In seabed areas with homogeneous relief (no significant variations in slope), fine-grained sediments typically result in weaker backscatter signals, while coarser sediments tend to produce stronger backscatter responses.

The identified morphologic features were manually traced on a final morphological map, based on the information provided by the three aforementioned maps (DEM, slope and backscatter). Gullies were automatically extracted from the underwater drainage network QGIS tool, verified, and subsequently mapped. Two types of gullies were identified based on the Tubau et al. (2013) classification: rim gullies and toe gullies. Rim gullies are characterized by large, well-developed gullies with sharp boundaries that are typically closely spaced and develop

a dendritic morphology that commonly extend from the thalweg to the canyon rim. Conversely, toe gullies are smaller in size, with a straight pattern and appear at the lower areas of the canyon flank. For the accurate plotting of the canyon axis and rim, the deepest and highest point, respectively, were extracted from equidistant lines (100 m) perpendicular to the canyon axis in Globbal Mapper.

4. Results

The Blanes Canyon was divided in three different areas in order to simplify the visualization of its morphological features (Fig. 3A). They include: the "canyon head" corresponding to the shelf-incised sector, the "upper canyon" for the sector comprising a large tributary channel, and the "middle canyon" from where the tributary channel converges with the main axis to the depth where the gullies vanish. The "lower canyon" corresponds to the deepest part of the Blanes Canyon, which is outside the study area. There, the canyon evolves into a submarine channel following a pattern of large meanders until it finally reaches the Valencia channel at ~2600 m water depth (Amblas et al., 2004; Canals et al., 2004, 2013).

The thalweg of the Blanes Canyon shows a concave and monticulate longitudinal depth profile, showing knickpoints at different depths (Fig. 4). The eastern rim longitudinal profile of the canyon remains practically flat until it reaches the shelf break, where an abrupt change in depth (140 m drop) occurs. This step leads in depth to a concave profile that becomes slightly convex in the middle canyon. The western rim longitudinal profile shows a sigmoidal shape. Both rims show similar depths in the canyon head sector. The western flank is significantly shallower than the eastern flank (maximum depth difference of 250 m) over much of the upper and middle canyon sectors, but at ~600 m depth, the trends of the longitudinal profiles of both rims reverse, resulting in an increasingly deeper western rim. The longitudinal profile of the eastern tributary thalweg is slightly concave and monticulate intersecting with the main thalweg at ~1600 m depth. Several knickpoints appear where the thalweg shows major steps (Fig. 4).

The cross-sectional view of the canyon displays the typical "V-shaped" profile of canyons incising the shelf break (Fig. 4). The canyon head transversal profiles reveal vertical walls in the most incised areas, mainly found adjacent to the axis in the canyon head sector (Fig. 3C). The highest wall in the whole canyon (385 m elevation) is located at the transition between the canyon head and the upper canyon sector (P3). This same profile crosses the irregular eastern flank and shows two zones with vertical walls, the highest of which coincides with the head of the tributary channel incision. Deeper, the cross-section of the middle canyon displays a very open V-shape, exposing a broader axis with the two canyon rims found at different depths.

4.1. Canyon head

The canyon head comprises the shelf-incised area from the canyon tip, located at 70 m water depth, to ~1200 m axial depth and it has a total length of 20,175 m (Fig. 5 and Table 2). The canyon head starts with a NE-SW trend orientation, parallel to the coastline (Fig. 1), but sharply turns to an almost N-S orientation at ~600 m axial depth. In this abrupt turn, the occurrence of a pronounced axis incision is particularly noticeable, resulting in a gorge bordered by high vertical walls (see Section 4.4.1). Deeper down, the thalweg displays a sinuous profile covered by cyclic steps, with frequent occurrence of terraces along the axis at the bases of both flanks (Fig. 5D), and features an ever-widening axis (max. 750 m wide) and high backscatter (Fig. 5B).

The canyon head is characterized by an eastern flank that exhibits a gentle slope (5° to 15°) and in the northern sector, it is characterized by the absence of any evident morphological features (Fig. 5D). Down-canyon, the slope increases and slide scars appear, occasionally revealing prominent scarps (Fig. 5C and D). Deeper than 800 m axial depth, toe gullies dominate the eastern flank, particularly where the

slope exceeds 20°. These toe gullies display a high backscatter axis (Fig. 5B), and have maximum lengths of 2859 m (Table S1). They are interrupted by different levels of escarpments with gradients steeper than 50°, and stop their retrogression at a large escarpment that extends along the 400 m isobath (Fig. 5C and D). Shallower than this 400 m isobath, the eastern flank displays a featureless and fairly gentle slope (5°-10°).

The western rim is narrow and steep over its first 500 m, but it becomes wider and gentler as the canyon turns to an NNE-SSW orientation (Fig. 5A and C). Down-canyon, the western rim presents a featureless character and gentle slope values (5° to 10°) in its shallower sector that suddenly increase towards the canyon axis, reaching general values >20° (Fig. 5C and D). This sudden change in slope values was mapped as a continuous slope break (Fig. 5D). The western flank lacks evident morphological structures until it reaches ~850 m axial depth, where an area with vertical walls appears (see Section 4.4.2). Toe gullies with maximum lengths of 1765 m develop above these walls, without reaching the slope break (Fig. 5D and Table S1). The deepest sector of the western flank is carved by high backscatter rim gullies (minimum length of 2470 m) that generally reach, and locally surpass, the slope break (Fig. 5A, B and Table S1), and gradually increase in size down-canyon (Fig. 5D). Scarps with slopes of >50°, corresponding to small canyon walls of varying size (from a few meters to hundreds of meters), extend along different isobaths interrupting the path of these rim gullies (Fig. 5D). The largest vertical wall in the canyon is on the western flank at 1200 m axial depth next to the thalweg, with an elevation of 385 m (Figs. 4, 5A, C and Table S1). This wall coincides with the limit of the canyon head region and displays a sharp bend at the confluence of the main canyon thalweg and the wall of a major rim gully on the western flank.

4.2. Upper canyon

The upper canyon comprises the sector of the canyon in which the direction of the canyon axis turns to NNW-SSE, showing a rectilinear pattern that extends along 13,918 m (Fig. 6A and Table 2). The canyon thalweg is wider than that in the canyon head sector (minimum width of 475 m at its shallower part and increasing down-canyon reaching a maximum of 1273 m) and is covered by a field of 9 cyclic steps (Fig. 6C and Table 2). This canyon sector comprises a major meandering tributary channel (21,128 m) incising the eastern canyon flank and reaching the shelf break. The confluence of this tributary with the main canyon axis at axial depths of ~1600 m displays the sector of the axis with the maximum width (1400 m) and marks the end of the upper canyon sector (Fig. 6A and Table 2). The tributary thalweg is 450 m wide on average in its head, and widens with increasing depth, reaching >700 m in its middle course and a maximum of 1314 m at the confluence with the main canyon axis (Fig. 6A and Table 2). The tributary channel thalweg is also covered by 12 cyclic steps (Fig. 6B and C), and at ~600 m axial channel depth, the tributary undergoes a strong axial incision, exposing a group of vertical walls topped by terraces (see Section 4.4.3).

The eastern canyon rim on the upper canyon sector shows a preferential *E*-W direction where it coincides with the shelf break (Figs. 1 and 6A), displaying an abrupt change of slope (Fig. 6B). On the upper continental slope, the eastern canyon rim turns towards the SW, becoming the canyon interfluve (Figs. 6C and 1A). The eastern flank is largely featureless in its shallower (i.e., upper slope) part, displaying gentle gradients <15° (Fig. 6B and C). At greater depths (>600 m), the smooth slope of the eastern flank is interrupted by the presence of several scarps and partially buried escarpments with gradients >50° (Fig. 6B and C). Discontinuous groups of toe gullies are confined to the lower areas of the eastern flank, close to the main canyon and tributary thalwegs, in regions where the slope gradients are >30°. Additionally, a large amphitheater-shaped slide scar (11,156 m) with toe gullies (minimum length of 913 m) in the deeper and steeper part is found southward of the most pronounced bend of the tributary channel, slightly deeper than the
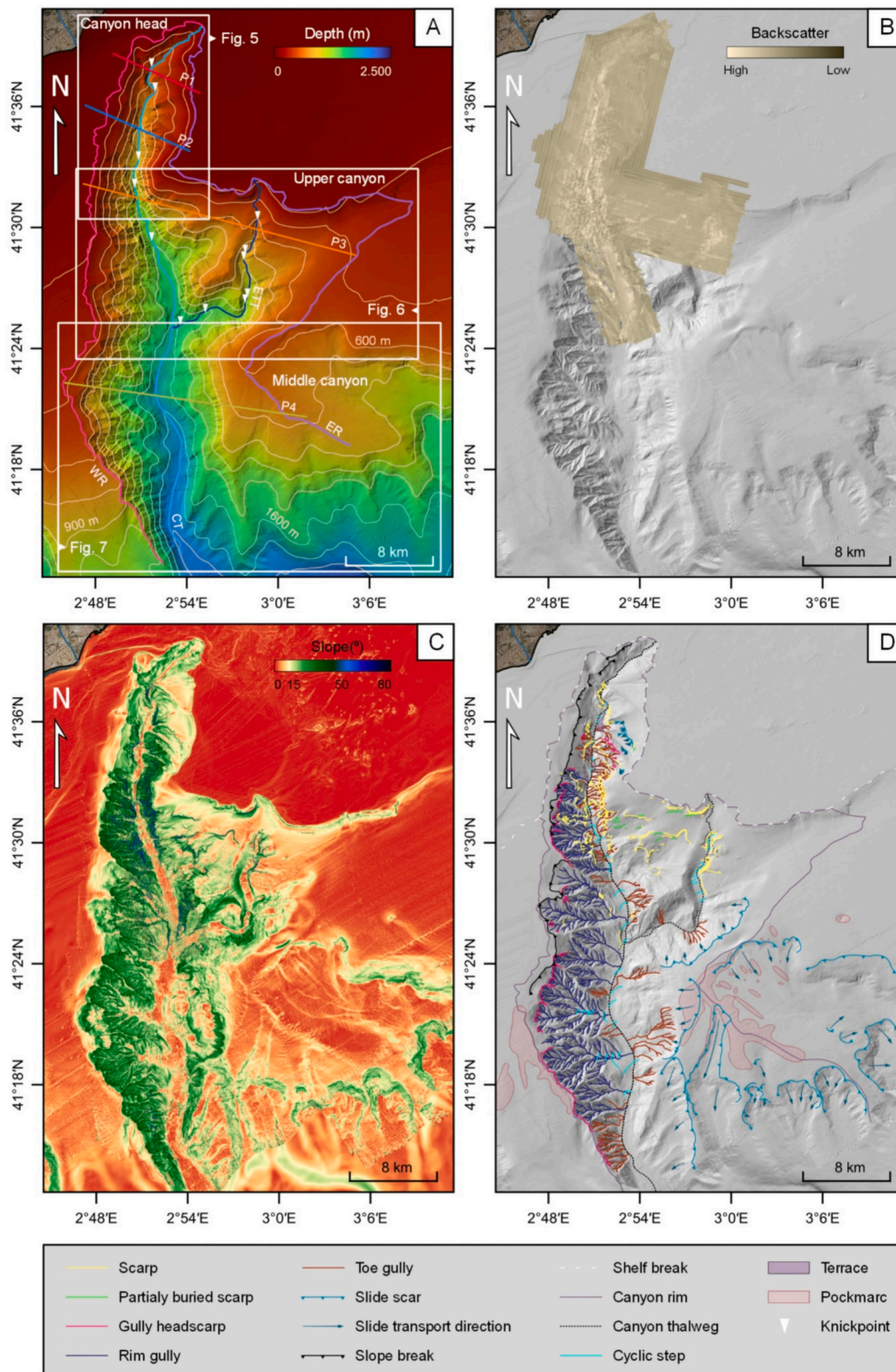
Fig. 3. Blanes Canyon map; canyon head, upper and middle reaches. (A) Shaded relief map with 200 m contour lines showing the different sectors in which the canyon has been divided, and the location of the bathymetric profiles illustrated in Fig. 4 (ER: Eastern rim, WR: Western rim, CT: Canyon thalweg, ETT: Eastern tributary thalweg and P1-P4). (B) Backscatter map. Light colors represent higher intensity values offered mainly by the rocky substrate and steep slopes, while dark colors represent lower intensity values typical of fine-grained sediment, sand and gentle seafloor areas. (C) Slope map measured in degrees. The blue colors show slope values of >50° matching the escarpments. (D) Geomorphological map of the canyon, showing the morphologic features visible at canyon scale as well as the underwater drainage network inferred from the three aforementioned maps.
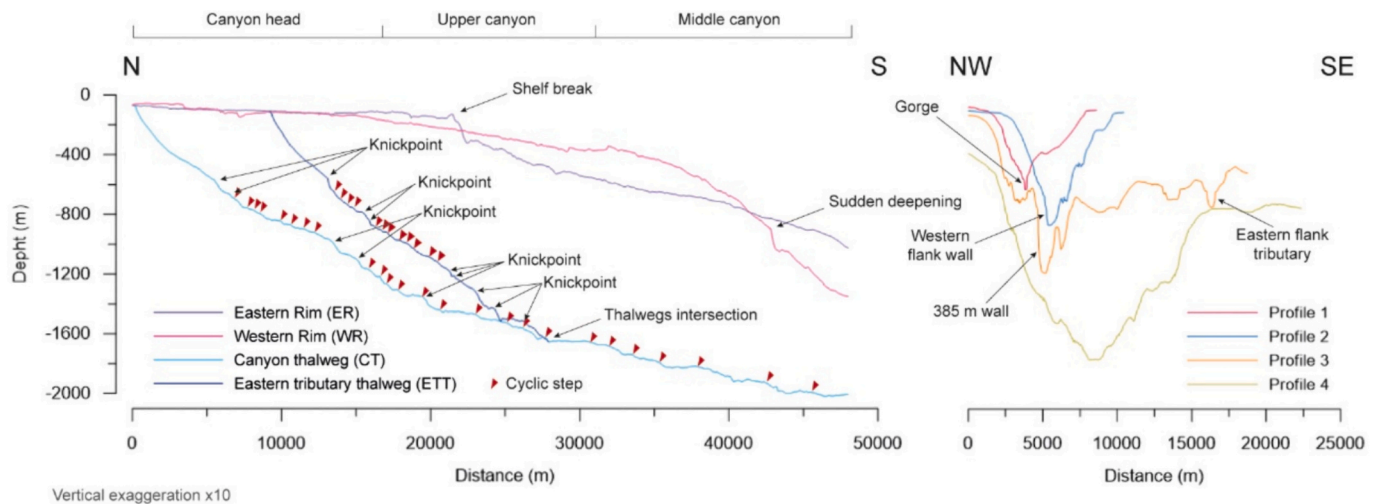
Fig. 4. Longitudinal (left) and transversal (right) profiles of the Blanes Canyon (see location in Fig. 3A). Longitudinal profiles correspond to the canyon thalweg and both eastern and western rims, from the tip to the end of middle canyon sector, with the exception of the eastern tributary channel. The transverse profiles P1 to P4 (see their location in Fig. 3) have been taken across the canyon head, the upper canyon and the middle canyon sectors, showing the vertical walls in the gorge, the western flank and the eastern flank tributary.

canyon interfluve (Fig. 6D and Table S1).

The western flank displays a completely different morphology than the eastern flank and it is entirely carved by rim gullies with maximum lengths of 10,374 m (Fig. 6A and Table S1) that generally finish at the slope break, generating a gully headscarp, although the most developed gully reaches the western canyon rim (Fig. 6B and C). However, similar to the canyon head region, between the slope break and the western canyon rim, there is a flat area with gradients ~5°, occasionally reaching 15°. Several isolated toe gullies (maximum length of 2633 m) also appear interspersed in the shallow parts of the western upper canyon flank, ending at the base of steep (>50°) scarps (Fig. 6C and Table 2).

4.3. Middle canyon

The middle canyon thalweg follows a slightly sinuous (1.09) N-S orientation and extends from 1700 m to 2000 m depth along 22,266 m (Fig. 7A and Table 2). The axis of the canyon widens (maximum width of 2160 m) and is covered by 6 cyclic steps that disappear at 1900 m axial depth (Fig. 7B, C and Table S1). Contrary to the thalweg orientation, the eastern and western canyon rims are WNW-ESE and NW-SE oriented respectively, accompanied by pockmark fields whose distribution is aligned in the same direction (Fig. 7C). The rims orientation causes the western flank to become increasingly narrower down-canyon and the eastern increasingly wider.

The eastern flank in the middle canyon sector displays very gentle slopes (0° to 10°) and is carved by six amphitheater-shaped slide scars (maximum length of 23,383 m) (Fig. 7C and Table S1) that increase the gentle slope values to >15° at the slide head-scar region (Fig. 7A and B). The south-facing slide scars appear to roughly follow the 1200 m iso-baths, although one slide progressed shallower than the others until reaching the eastern canyon rim and a pockmark field. Toe gullies (maximum path of 7098 m) develop in the northern sector of the middle canyon eastern flank, in areas where the slope exceeds 20° (Fig. 7B), without reaching a wide slide scar, which is also coincident with a pockmark field aligned with the eastern canyon rim.

The western flank of the middle canyon sector, similar to the upper canyon sector, is entirely carved by rim gullies, including the most developed ones of the entire canyon (maximum length of 10,572 m) (Fig. 7C and Table S1). Some gullies reach the slope break in the northern shallower section and the canyon rim in the southernmost deeper section. Two of the largest gullies present a broad, flat

downstream axis before merging with the main canyon thalweg, and are each affected by 4 cyclic steps (Fig. 7B, C and Table S1). Few isolated toe gullies with maximum lengths of 4152 m also appear intercalated between the major rim gullies and dominate the south of the section, in accordance with the narrowing of the western flank (Fig. 7A, C and Table S1) and reduction of its height with increasing depth (Fig. 4).

4.4. High resolution view of vertical canyon walls

Fine-scale morphologic features of three regions of the Blanes Canyon with presence of vertical walls were mapped at very high-resolution (80 cm) using the H-ROV *Ariane*. Those regions were located at the canyon head gorge, at the base of the western canyon flank, and at the head of the eastern flank tributary (Fig. 2), and are described separately in the following sections.

4.4.1. Canyon head gorge

The surveyed canyon head gorge (Fig. 8A) is found between 465 and 653 m depth in the upper canyon head region (Fig. 5A). It shows a U-shaped sinuous axis, limited by the presence of large vertical walls topped by sharp escarpments along both sides of the axis. The walls are easily recognizable at broad- and fine-scales (see Profile 1 section in Fig. 4) due to their high elevation (reaching up to 80 m). They exhibit high backscatter (Fig. 8B) and maximum slopes of 88 degrees (Fig. 8C). The axis starts in the shallowest part of the gorge with an extremely narrow (22 m minimum width) incised left turning bend that excavates the lower reaches of the western canyon flank (Table 2). It continues down-canyon with a much wider (130 m maximum width) right turning bend that leads to the widening of the thalweg and excavates the lower reaches of the eastern canyon flank. At the entrance of this second bend, the canyon axis bifurcates, leaving a small terrace at 620 m axial depth on its central part. A field of small-scale furrows, incised down into fine-grained sediments, following the flow direction and with a length of ~180 m is found on the central part and exit of the bend (Fig. 8A and D). The furrows display centimeter-scale amplitudes and wavelengths and are easily recognized in the ROV images (Fig. 9A). A small contouritic moat bounded by groups of small blocks from rock falls runs at the base of the western wall, following the direction of the furrows field (Fig. 8D). Down-canyon, the canyon axis narrows to reach 100 m wide at axial depths of 630 m, following a straight path in NNE-SSW orientation, and deeper, the large vertical walls diverge and become more separated widening the canyon, although the axis maintains a narrow thalweg
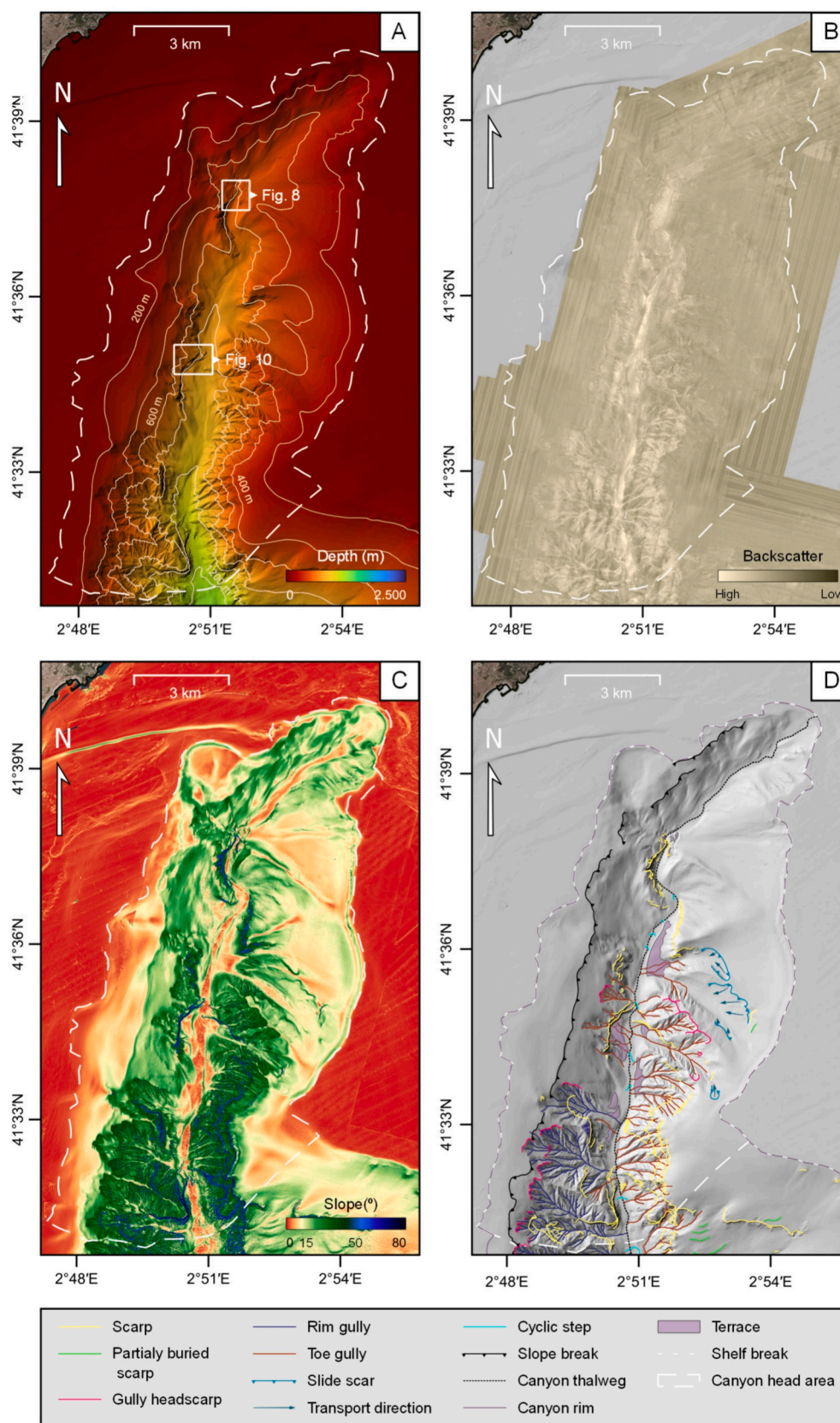
Fig. 5. Blanes Canyon head sector. (A) Shaded relief map with 200 m contour lines showing two of the surveyed regions with vertical walls. (B) Backscatter map. Light colors represent higher intensity values offered mainly by the rocky substrate and steep slopes, while dark colors represent lower intensity values typical of fine-grained sediment, sand and gentle seafloor areas. (C) Slope map measured in degrees. The blue colors show slope values of >50° matching the escarpments. (D) Geomorphological map of the canyon, showing the morphologic features visible at canyon scale as well as the underwater drainage network inferred from the three aforementioned maps.

Table 2

Morphometry of the three sectors (canyon head, upper canyon and middle canyon) and the tributary channel of the Blanes Canyon.

Morphometry	Canyon head	Upper Canyon	Middle Canyon	Tributary channel
Thalweg length (m)	20,175	13,918	22,266	21,128
Thalweg straight length (m)	17,400	13,058	20,343	15,818
Thalweg sinuosity index	1.16	1.07	1.09	1.34
Maximum thalweg width (m)	750	1400	2160	10,314
Minimum thalweg width (m)	22	475	632	40
Eastern rim length (m)	15,739	47,021	23,676	
Western rim length (m)	25,528	13,412	27,761	
Max. High Eastern rim (m)	980	1325	1135	
Min. high eastern rim (m)	0	1130	690	
Max. high western rim (m)	970	1310	1350	
Min. high western rim (m)	0	1095	670	
Max. rim to rim width (m)	8739	30,828	26,092	
Min. rim to rim width (m)	476	12,046	14,525	
Area (m^2)	115,164,831	318,794,700	407,944,014	

incision (~100 m wide) bounded by relatively small cliffs (max. 15 m high) (Fig. 8A and D). In this sector of the canyon axis, a field of ripples was observed on the ROV footage, oriented perpendicular to the axis direction (Fig. 9B).

The eastern flank developed above 70 m high vertical walls, showing a considerable slope (10° to 30°), which is carved by many small gullies and emerging gullies (Fig. 8C and D). The term "emerging gully" has been used here to define very small (50 m average length) and straight channels with an incision less or around 1 m (i.e. green arrows in the legend of Fig. 8D). They were mapped only in the limits of the shallowest bend (Fig. 8D). The small gullies flow into the canyon axis incising the flank with a slightly curved path, except the striking meandering small gully, ending above the second bend of the gorge (Fig. 8D). The incisions of both the small and the emerging gullies uncover a large number of scarps (> 50° slope) and partially buried scarps (> 30°) (Fig. 8C and D), displaying high backscatter values (Figs. 8B).

The western flank developed above 80 m high vertical walls showing rocky outcrops with parallel stratification, where cold-water corals attach and develop (Fig. 9C). This flank shows a single small gully flowing into the canyon where the first bend occurs (Fig. 8D). The western flank stands out for its terraced and highly stratified nature (Fig. 8A and D), showing terraces which are separated by partially buried scarps. The terraces primarily match with gentle slopes and low backscatter intensity, in contrast to the strata scarps (Fig. 8B and C). Above these terraces, an alignment of escarpments of great continuity is displayed, leaving visible >70° slope walls that could reach ~10 m in height (Fig. 8C and D). This alignment eventually merges down-canyon with the top of the southern main vertical walls, on which small emerging gullies observed in ROV images show an incision of ~50 cm (Fig. 9D).
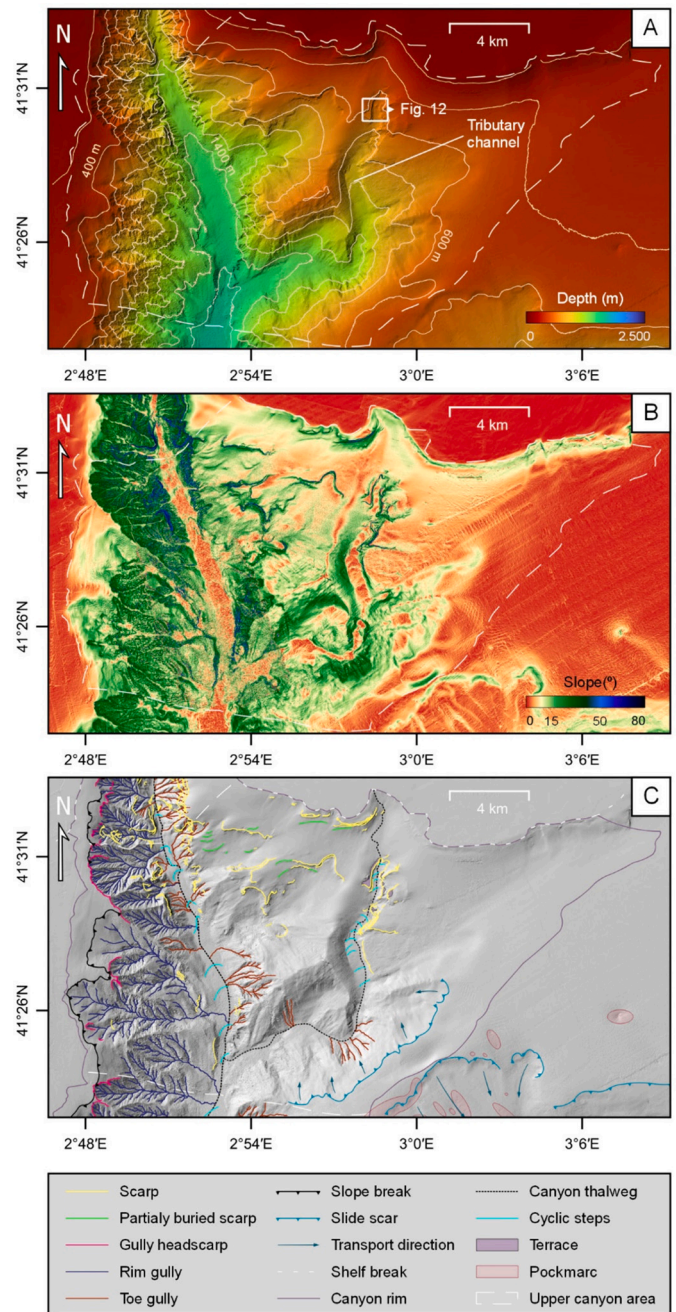

Fig. 6. Upper sector of the Blanes Canyon. (A) Shaded relief map with 200 m contour lines showing one of the surveyed regions with vertical walls. (B) Backscatter map. Light colors represent higher intensity values offered mainly by the rocky substrate, while dark colors represent lower intensity values typical of fine-grained sediment and sand. (C) Slope map measured in degrees. The blue colors show slope values of >50° matching the escarpments. (D) Geomorphological map of the upper canyon showing the morphologic features visible at canyon scale as well as the underwater drainage network inferred from the three aforementioned maps.

4.4.2. Western flank

The surveyed western flank area lies in a depth range from 603 to 869 m (Fig. 10A), within the central part of the canyon head sector (Fig. 5A). It is characterized by a NE-SW oriented steep terrain with a general slope of >20°, alternating terraces at different depths and rocky vertical walls up to 80 m height with maximum slopes of 88° (Fig. 10A and C), and some areas of overhanging walls identified during the ROV dives. These vertical walls are characterized by sub-horizontal stratified
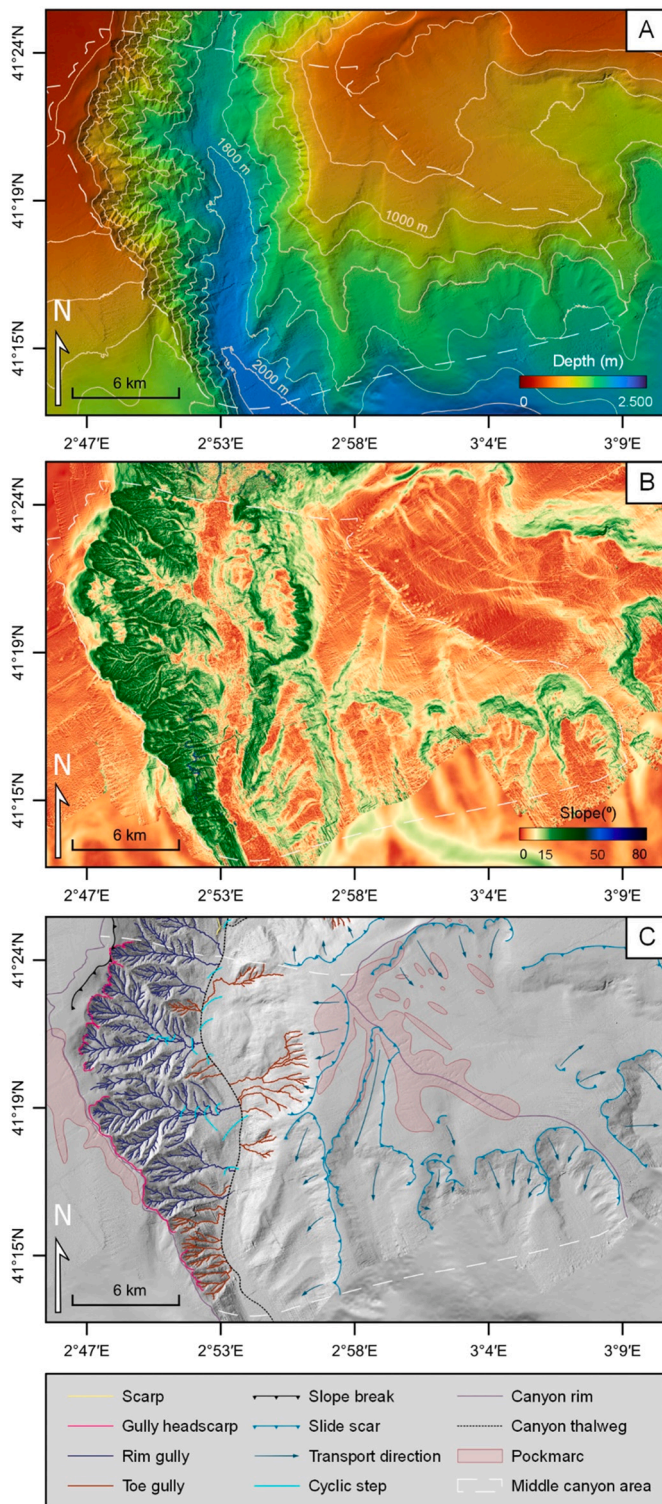
Fig. 7. Middle sector of the Blanes Canyon. (A) Shaded relief map with 200 m contour lines. (B) Backscatter map. Light colors represent higher intensity values offered mainly by the rocky substrate, while dark colors represent lower intensity values typical of fine-grained sediment and sand. (C) Slope map measured in degrees. The blue colors show slope values of >50° matching the escarpments. (D) Geomorphological map of the middle canyon sector showing the morphologic features visible at canyon scale as well as the underwater drainage network inferred from the three aforementioned maps.

outcrops that can be followed by the lateral continuity of high back-scatter lineations (Fig. 10B) also observed at ROV visual scales (Fig. 11A). The presence of falling blocks at the base of these walls is scarce. Instead, fine-scale spalling fractures could be observed on the walls during the ROV surveys (Fig. 11B). Strata scarps are disrupted by the presence of toe gullies, visible also at broad-scale (Figs. 5D and 10D), and by an abundant presence of high-intensity backscatter emerging gullies with average lengths of 38 m (Fig. 10B). Millimeter-wide linea-tions running downslope are also common in the ROV footage of the wall sediment surface, interpreted here as rills (Fig. 11C). Two large terraces can be distinguished on the northern sector of the surveyed canyon wall, which are excavated by moats bordering the base of the walls (Fig. 10A and D). On the shallower terrace, trawl marks caused by bottom trawling fishing activities can be observed, showing a predom-inant N-S direction. These trawl marks continue southwards along the main canyon axis, showing alternating medium-low backscatter in-tensities and with an excavation of <0.5 m and variable length (Figs. 10B and 11D).

4.4.3. Eastern flank tributary

The surveyed area from the Blanes Canyon eastern flank tributary channel covered a depth range between 527 and 768 m (Figs. 6A and 12A). It is a wide (500 m on average), U-shaped channel (see Profile 3 in Fig. 4) displaying an almost N-S orientation that excavates a gentle re-lief, leaving large terraces on both sides (Fig. 12A). The terraces develop at the top of distinctive high backscatter vertical (up to 87°) rockwalls that can be up to 70 m high (Figs. 12A to 12C). The tributary thalweg shows two cyclic steps, the shallower one coinciding with a small relief of 12.5 m with relatively high backscatter values and slope gradients (>30°).

The tributary eastern flank above the canyon wall has a stepped relief related to the underlying stratification and the presence of outcropping scarps (> 50°) and partially buried scarps (>30°). It is limited by an irregularly shaped eastern channel rim showing two large indentations, where the flank retreats, which coincide with areas at the adjacent tributary axis occupied by large falling blocks (>10 m long) of high backscatter (Fig. 12B and D). Accumulation of fallen blocks can be seen as well on the ROV footage under rectilinear sectors of the eastern tributary rim (Fig. 13A). Scars left by fallen blocks are also frequently observed on the ROV footage across the eastern flank vertical walls (Fig. 13B).

The tributary western flank, in contrast, displays a rim with a slightly curved trajectory and absence of large indentations and block failures (Fig. 12A). Instead, the base of the western flank is dominated by moats that follow the bathymetric contours. On the ROV footage conducted on this flank, scars left by falling flakes can be observed along the vertical walls (Fig. 13C). On top of the gentle terrace (< 5°) of the western tributary flank, a group of vertical walls (20 m high on average) is interrupted by two small gullies, which can be traced by steep gradients. A group of small, high backscatter blocks can be identified at the base of these walls, and are also visible through the ROV imaging (Figs. 12B and 13D).

5. Discussion

5.1. Tectonic control on the emplacement and evolution of the Blanes Canyon: Insights from broad-scale morphological evidence

Local tectonic structures such as faults, have a significant impact on the location, orientation, and geometry of many submarine canyons (Li et al., 2021). Rahiman and Pettinga (2006) attributed a tectonic influ-ence to canyons that do not follow a natural orientation controlled by gravitational flows along the maximum gradient and normal to the margin. The Blanes Canyon is obliquely oriented to the margin in its upper-middle reaches, being one of the most evident characteristics revealing its tectonic control. Although the Blanes Canyon margin
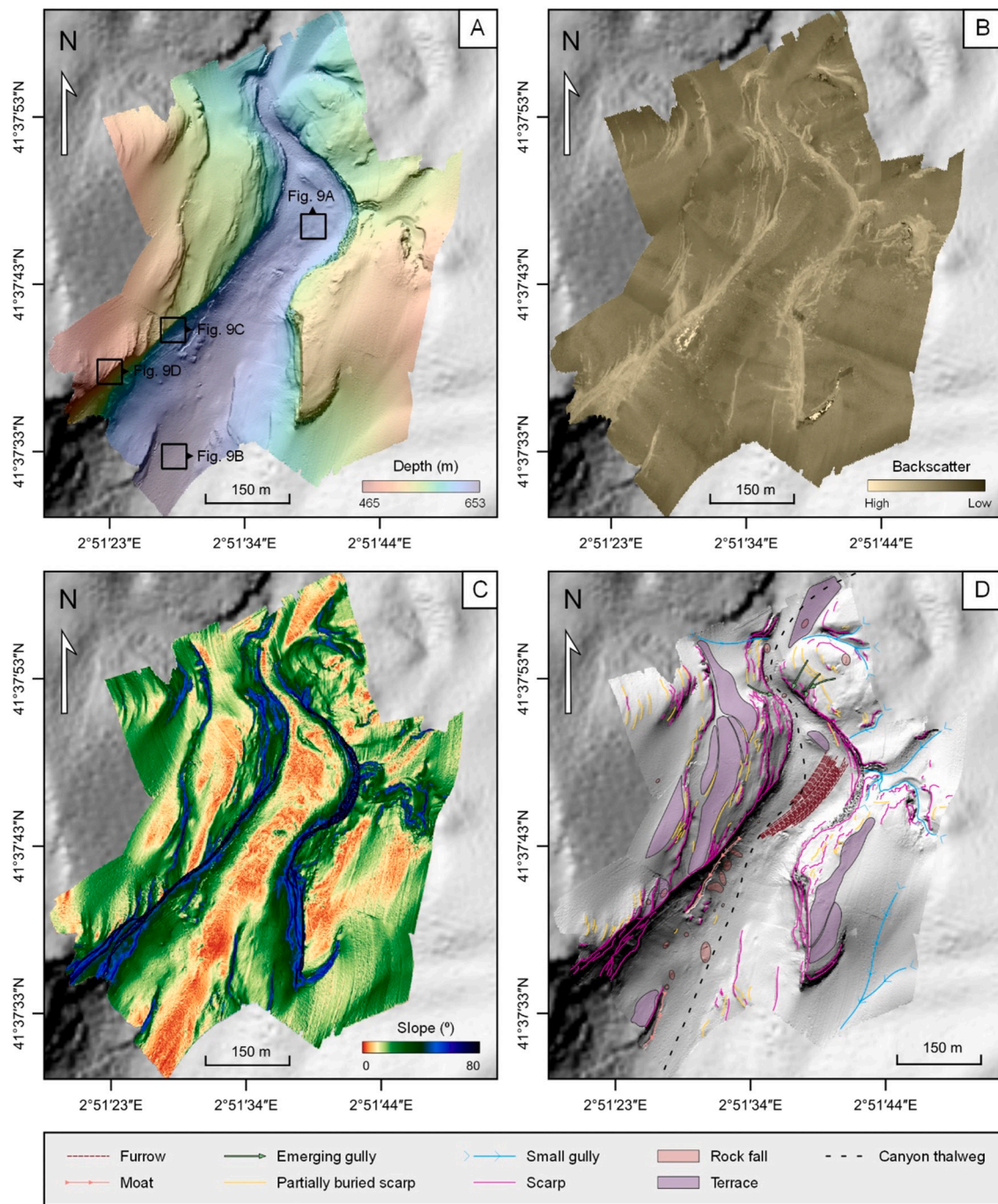
Fig. 8. Blanes Canyon head gorge, mapped at 80 cm resolution using the H-ROV *Ariane*. (A) Shaded relief map showing the location of the images acquired with the ROV *Liropus* in this region. (B) Backscatter map. Light colors represent higher intensity values matching with the vertical rockwalls. (C) Slope map measured in degrees. The blue colors show slope values of >50° coinciding with vertical walls. (D) Geomorphological map that shows the morphologic features visible only at this very fine-scale inferred from the previous three maps. Refer to supplementary material (Fig. S1) for a three-dimensional perspective of the maps.

currently lacks evidence of active tectonism in the area, its orientation coincides with several recognized subsurface fault systems (ITGE, 1989) and the path of the canyon axis is deflected in the intersection between fault systems, particularly the NE-SW and NW-SE systems (Fig. 1B). This is a common feature and can occur in all types of margins. Some examples in passive contexts are the abrupt direction changes controlled by faults that characterize the Slogget Canyon, in the northwestern Scotia sea (Palma et al., 2021) or the rectangular drainage morphology developed across growth faults in the Afam Canyon, in the onshore extensional zone of the Eastern Niger Delta (Mercier et al., 2023). Similar, in active margins, Naranjo-Vesga et al. (2022) related the

canyons orientation with structural lineaments in the Colombian Caribbean and Cerrillo-Escoriza et al. (2024) describe fault related bends of 90° in the thalwegs of Motril and Carchuna Canyons, in the Alboran sea. The general concave curvature of the Blanes Canyon thalweg (Fig. 4) suggests that the canyon has been dominated by marine erosion processes since the attenuation of the tectonic activity during the late Quaternary (Tassone et al., 1994), as observed by Gerber et al. (2009) in the Foix and Besòs canyons of the South Catalan margin. Nevertheless, the presence of knickpoints where the canyon deflects, and coinciding with steps (Figs. 3A and 4), would represent erosion-resistant strata but also the last remnants of the ancient fault systems.
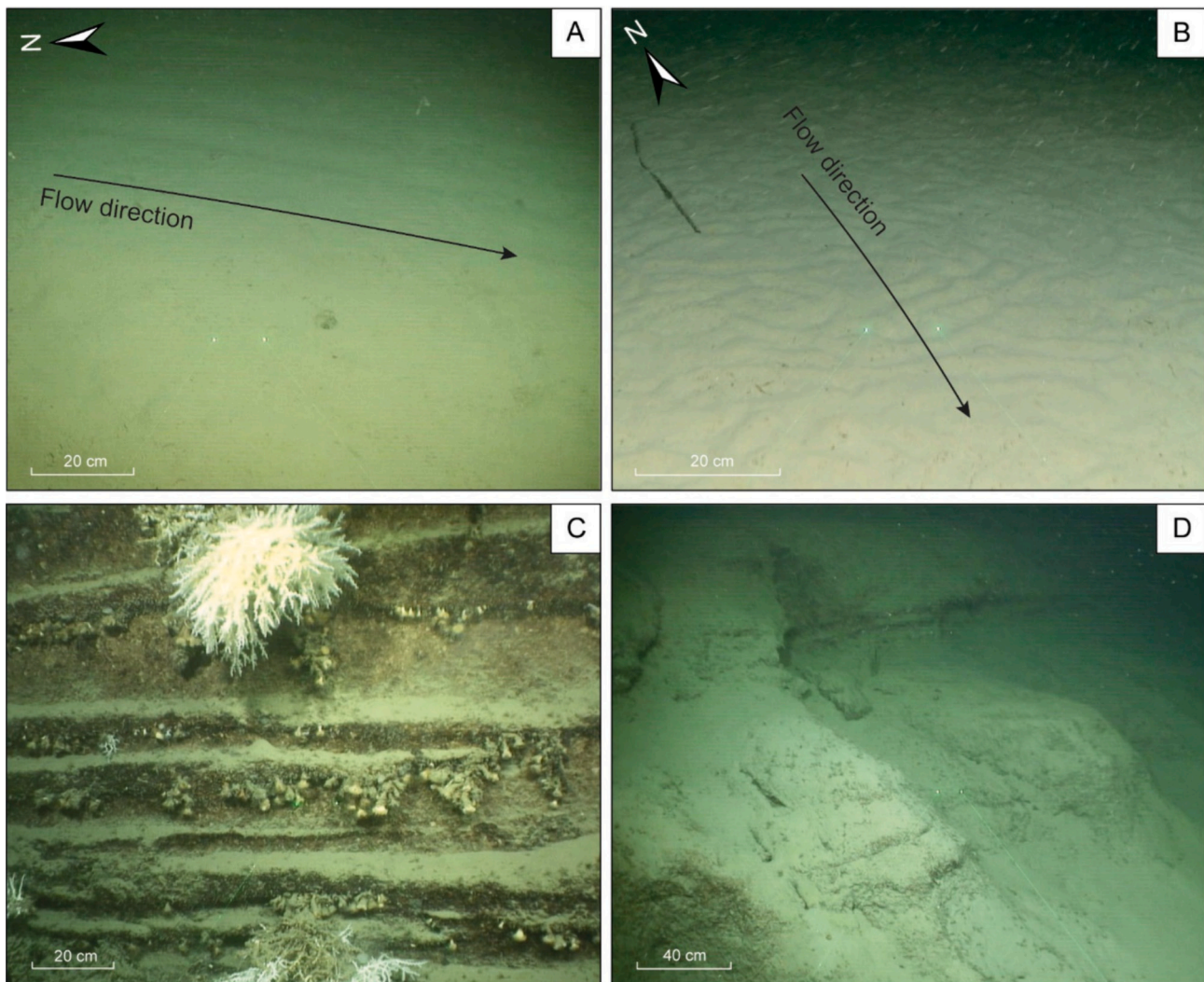
Fig. 9. Images extracted from the *Liropus* ROV HD video footage in the vertical walls of the gorge. (A) Field of small-scale furrows oriented parallel to the direction of the canyon thalweg, following the flow direction. (B) Ripples field perpendicular to the thalweg direction, the fortunate appearance of a *Posidonia oceanica* leaf confirms the flow direction. (C) Well-stratified vertical rockwall in which different types of cold-water corals (*Lophelia pertusa* and *Madrepora oculata*) are attached. (D) This image shows the onset of a channel created by erosion derived from sediment-laden gravity flows, here referred to as emerging gully. They show an incision of <1 m.

Knickpoints along the canyon axis have been associated with faults, altering the equilibrium of the longitudinal profile (Mitchell, 2006). Furthermore, the uneven topography of both canyon rims (Fig. 4) would also be related to the extensional fault system that defines the area, reinforcing the tectonic origin of the canyon. The shallower western rim represents the uplifted footwall, while the deeper eastern rim represents the subsided hanging wall. A similar morphology was observed in the Wairarapa (Mountjoy et al., 2009) and La Aguja submarine canyons (Restrepo-Correa and Ojeda, 2010) where the different relief topography of the canyon walls was explained by extensional fault systems.

A large number of morphological elements have been recognized accompanying the two buried fault systems in the area of the Blanes Canyon (Figs. 1B and 3D). Classical definitions such as of Shepard (1981) postulate that submarine fault valleys can be recognized by having V-shaped profiles with straight walls and the continuity of on-land fault valleys towards the sea. Transverse profiles on the Blanes Canyon (Fig. 4) support Shepard's definitions, since they show marked V-shaped incisions and vertical walls of up to 385 m in height. It is highly probable that the onshore Tordera River fault (Fig. 1B) connects offshore with the fault controlling the rectilinear portion of the main thalweg in the upper canyon sector (Fig. 6), giving weight to the

previously proposed definition.

Several morphologic features in the Blanes Canyon also provide further evidences of subsurface structures that could be associated to tectonism, such as pockmarks. Pockmarks with an aligned distribution related to buried tectonic features have been identified in the literature (Nakajima et al., 2014). In such cases, the over-pressured fluid tends to migrate vertically, along deeply buried faults, which are expressed at the surface as pockmarks fields (Davie and Buffett, 2003; Forwick et al., 2009; Riboulot et al., 2013; Riera et al., 2022). In the Blanes Canyon, the abrupt turn of the eastern canyon rim (from a NE-SW to a NW-SE direction) and the parallel western rim are coincident with two aligned pockmark fields (Figs. 3D and 7C), probably revealing the presence of buried faults. Additionally, the across-margin bathymetric profiles (Fig. 4) show a sudden deepening on the western rim. This step or sudden deepening is probably related to a normal fault whose dipping hanging wall corresponds to the deepest part of the rim, shortening the height of the west flank in this area. This latter evidence could explain the inaccuracy in the old fault system mapping (Fig. 1B), with the fault actually being located displaced in depth.
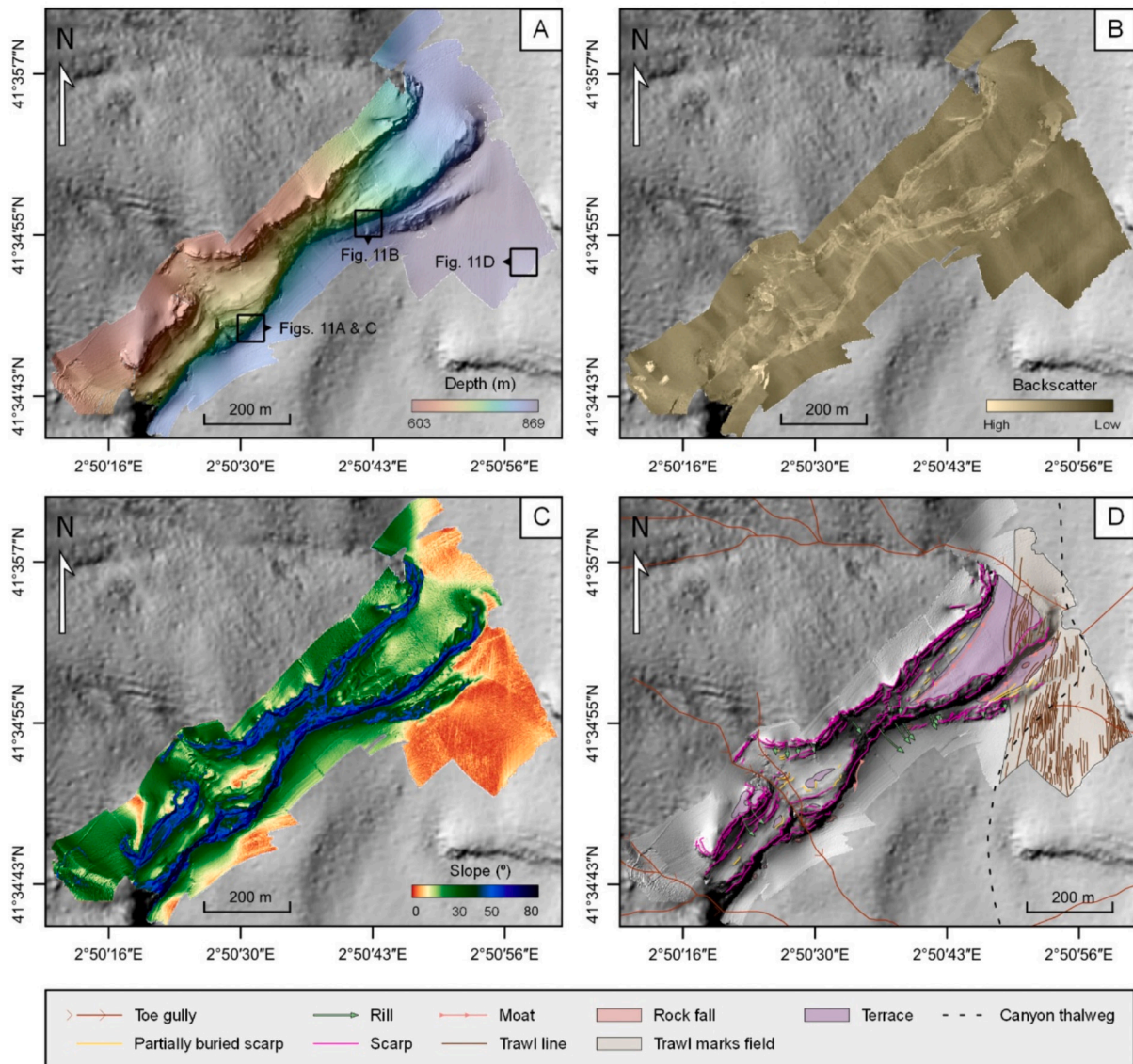
Fig. 10. Western flank area mapped at 80 cm resolution using the H-ROV *Ariane*. (A) Shaded relief map showing the location of the images acquired with the ROV *Liropus* in this region. (B) Backscatter map. Light colors represent higher intensity values matching with the vertical rockwalls. (C) Slope map measured in degrees. The blue colors show slope values of >50° coinciding with vertical walls. (D) Geomorphological map that shows the morphologic features visible only at this very fine-scale inferred from the previous three maps. Refer to supplementary material (Fig. S2) for a three-dimensional perspective of the maps.

5.2. Importance of stratigraphic control in shaping the broad-scale morphology of the Blanes Canyon

Axial incision, gully formation, and mass wasting are the main processes in widening submarine canyons and are important features in the transfer of sediment across and down-canyon (Baztan et al., 2005; Dowdeswell et al., 2008; Tubau et al., 2013; Wan et al., 2022). These processes do not necessarily act individually, but can interact between them (Baztan et al., 2005; Micallef et al., 2012).

The Blanes Canyon shows two asymmetric and clearly differentiated flanks: a gentle eastern flank, dominated by slides and toe gullies in the most incised areas; and a steeper western flank, dominated by networks of rim gullies (Figs. 3 and 14). Both processes, gully formation and sliding, are commonly closely related to the steepness of the flanks (Kenyon, 1987; Sultan et al., 2004; Fedele and García, 2009; Scarselli, 2020). In the Blanes Canyon, however, the resulting differentiation between morphologic features seems to be related to the bedding-slope relationship. The Blanes Canyon is incised into a Miocene-Plio-Quaternary stratigraphic sequence mainly dipping to the SW (ITGE,

1989; Lastras et al., 2011). The eastern flank shows the dip of the strata in the same direction as the slope flank, making it a cataclinal slope. Conversely, the western flank is characterized by an orthoclinal to anaclinal slope, since the dip of the strata is displayed in a direction from orthogonal to opposite with respect to the slope of the flank (Fig. 14). Cataclinal slopes are the most slide-prone landscape, since stratification planes constitute a potential pre-conditioning factor as they act as planes of weakness (Grelle et al., 2011). It is common for slides associated with cataclinal slopes to be translational, decreasing the slope gradient of the flank (Varnes, 1978; Micallef et al., 2012). This would explain the gentle slope on the eastern flank and its susceptibility to slides, probably to be translational.

The highest concentration of slides occurs associated to the pockmark fields (Fig. 3D), suggesting that the occurrence of fluid escape, in combination to the cataclinal slope type, could have acted as a potential driver of slides in the Blanes Canyon. Riboulot et al. (2019) already showed that the occurrence of pockmarks plays an essential role in inducing slope instabilities in the submarine slide on the outer-shelf and slope of Nigeria. The slides and the smooth relief on the Blanes Canyon
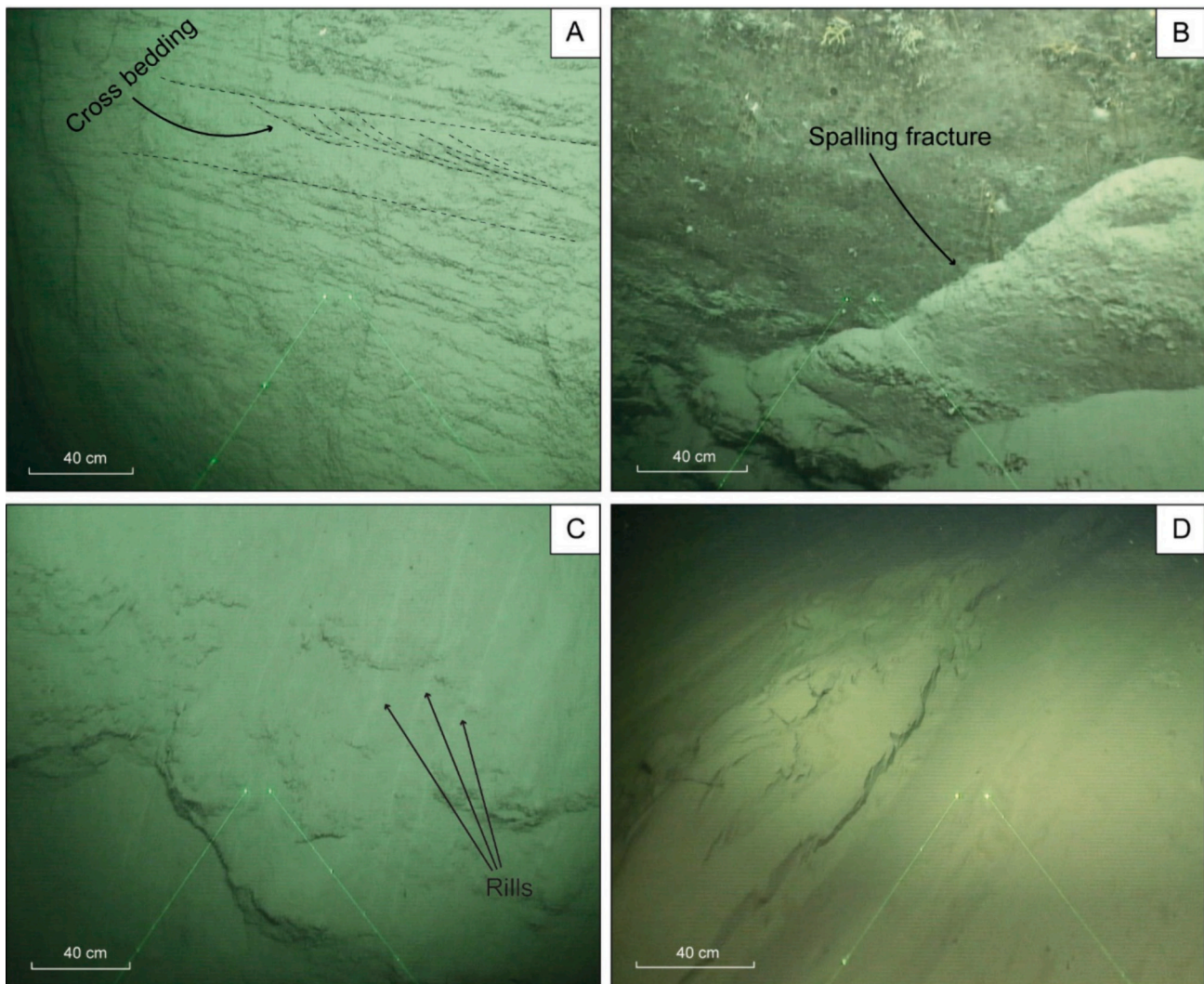
Fig. 11. Images extracted from the *Liropus* ROV HD video footage in the vertical walls located on the western flank. (A) Cross-bedded strata revealing a high degree of stratification even at outcrop scale. (B) Flake-like fractures (spalling fracture) resulting from the backward retreat of the cliffs. (C) Small lineations or rills flowing in the direction marked by gravity forces, the evolution of these tiny morphologic features evolves by embedding themselves in the seabed to form emerging gullies (Fig. 9D). (D) Morphology left by trawl gear, known as trawl mark.

eastern flank were reinforced by axial incision resulting from episodic turbidity currents undermining the flank, as is the case in other submarine canyons (Pratson and Coakley, 1996; Baztan et al., 2005). The upwardly concave longitudinal profile of the thalweg in Blanes (Fig. 4) fits with the theory of Gerber et al. (2009) and Soutter et al. (2021), which denotes that an upwardly concave canyon longitudinal profile is indicative of a canyon dominated by erosion through turbidity currents rather than being dominated by sediment deposition or tectonic deformation. In addition, sliding in the Blanes Canyon would have provided material to the canyon axis and in its way downslope was transformed into debris flows and/or turbidity currents as already observed in other cases in submarine canyons (Normark and Piper, 1991; Rahiman and Pettinga, 2006; Bernhardt et al., 2015). The slide material on the axis most likely descended downstream thanks to the episodic gravity currents, contributing to axial incision and ongoing canyon widening. This hypothesis is strengthened by the train of cyclic steps found along the canyon thalweg with no evidence of activity (Figs. 3 and 4), which represent the reworking of slide material under episodic events of turbidity currents, comparable to what happens in the San Mateo canyon-channel system (Covault et al., 2014).

The western flank is subject to an orthogonal to anaclinal slope (Fig. 14). This slope, in contrast to the eastern flank, allows the gradient

to remain higher, as the planes of weakness dip obliquely and opposite to the slope face. Micallef and Mountjoy (2011) postulate that, for submarine gullies to occur in submarine canyons, a high gradient that enhances sediment entrainment and flow concentration is of major importance, but in addition a tractive force must exist. Accordingly, the evolution of material derived from down-sliding could act as a tractive force in the initiation of the formation of gullies. Rim gullies in the Blanes Canyon probably originated after the slides. The material of these slides facilitated sediment entrainment, generating small gullies at the foot of the flank that evolved up slope to reach their present configuration. These gullies are similar to those found in the Nazaré Canyon, offshore Portugal (Masson et al., 2011), where they remain in time and act as another way of sedimentary input to the thalweg. The presence of toe gullies at the foot of the eastern flank slides (Figs. 6C and 7C), where the steepest slopes appear in connection with axial incision, further confirm this theory.

The rim gullies on the western flank show a clear trend of down-canyon growth and, after reaching their maximum size, from approximately 34 km down-canyon, they decrease in size again (Fig. 3A and D). Toe gullies appear in the southern section. The depth difference between the longitudinal profiles of the canyon thalweg and the western canyon rim (Fig. 4) fits perfectly with this trend, as the separation between both
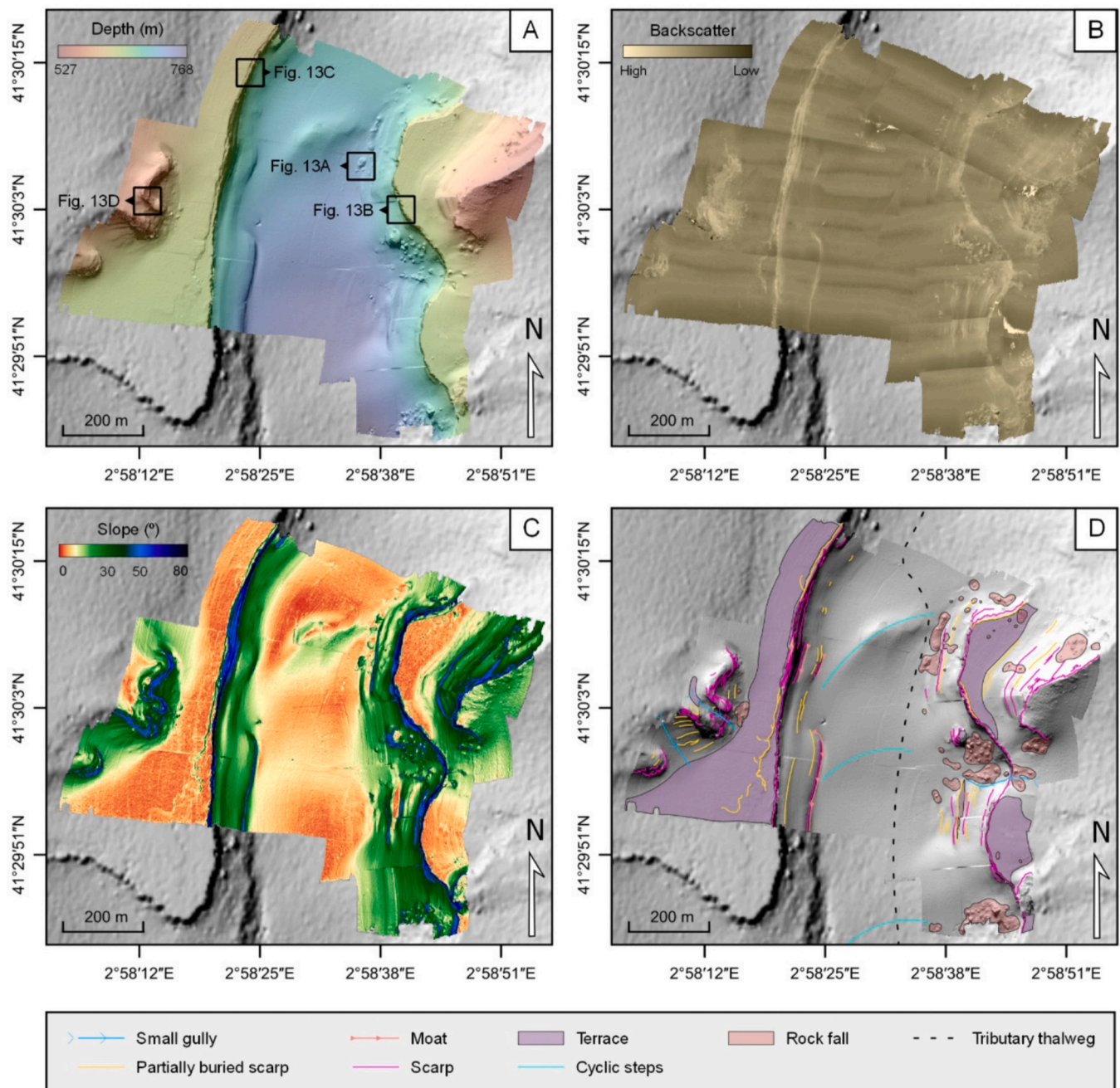
Fig. 12. Eastern flank tributary mapped at 80 cm resolution using the *Ariane* H-ROV. (A) Shaded relief map showing the location of the images acquired with the ROV *Liropus* in this region. (B) Backscatter map. Light colors represent higher intensity values matching with the vertical rockwalls. (C) Slope map measured in degrees. The blue colors show slope values of >50° coinciding with vertical walls. (D) Geomorphological map that shows the morphologic features visible only at this very fine-scale inferred from the previous three maps. Refer to supplementary material (Fig. S3) for a three-dimensional perspective of the maps.

profiles (or the height of the western flank) is greater in depth, peaking where the largest rim gullies of the Blanes Canyon appear. García-García et al. (2012) compared the size of the gullies with their maturity, with the largest being the most mature. In this way, the height of the western flank in Blanes Canyon is directly related to the maturity of the rim gullies. Toe gullies appear in the deepest sector where the western flank height is lower, slowing down the development of the gullies and not allowing the growth of a dendritic network even if the gullies reach the canyon rim.

5.3. Revealing canyon wall processes from fine-scale morphological evidence

The development of canyon walls in the Blanes Canyon is closely related to the axial incision following the inherited structure of the two fault systems prevalent in the region. This structural arrangement not only results in the formation of the canyon's steepest terrain but also exposes a distinct stratification that is perceptible across a wide range of scales, from broad- to fine-scale.

Axial incision follows the alignment of the NE-SE fault system in two of the mapped areas with vertical walls (Figs. 10 and 12). The gorge area deviates from this pattern as an interplay between two fault systems, NE-
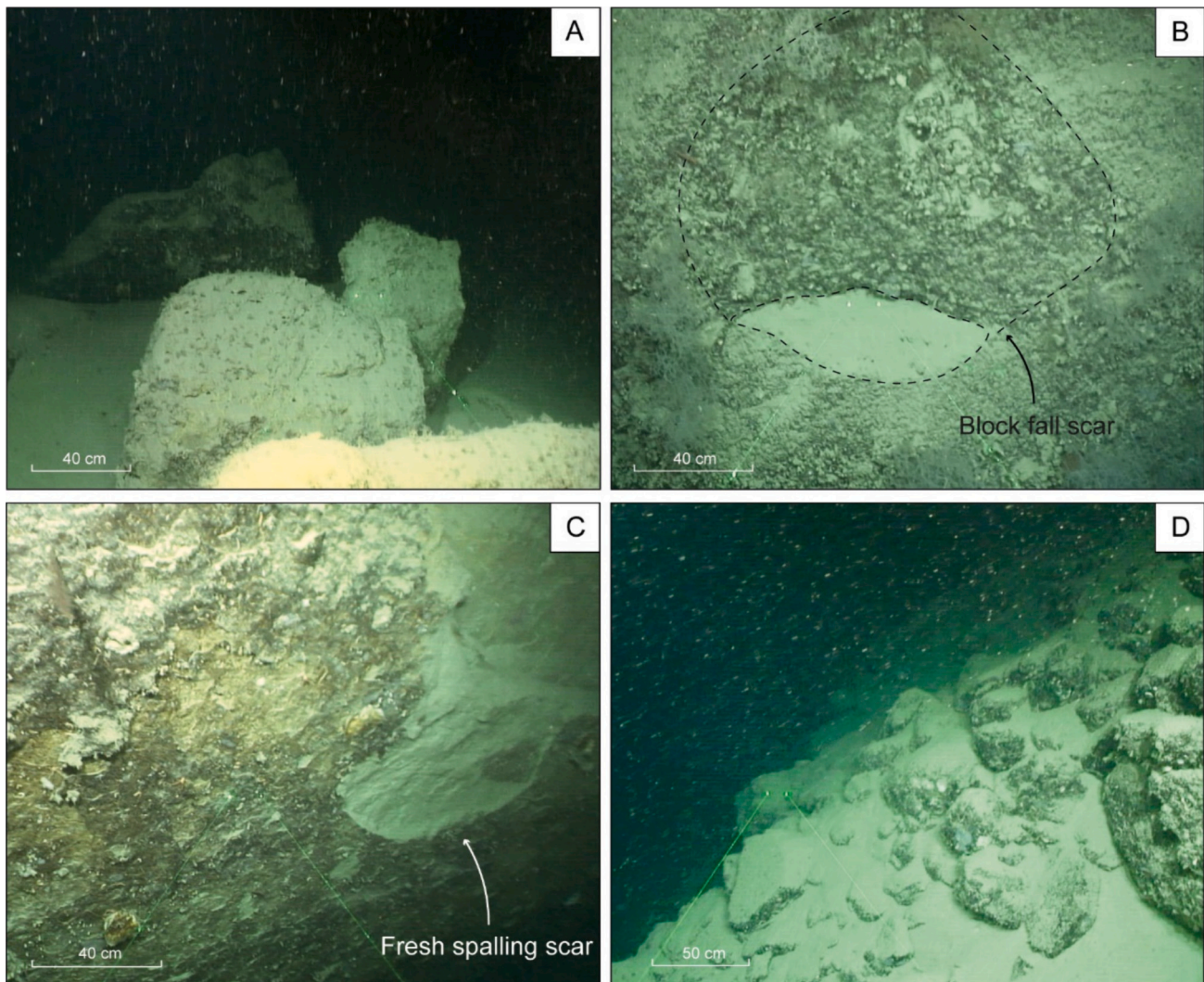
Fig. 13. Images extracted from the *Liropus* ROV HD video footage in the vertical walls from the eastern flank tributary. Large rocky blocks deposited on the axis from erosion on vertical walls (A) and an example of the scars they leave behind (B). (C) Scars left by the wall retreatment process of spalling failure. (D) Field of small blocks covering the seafloor derived from erosional fallout from vertical rock walls.

SW and NW-SE, leads to the formation of two pronounced meanders (Fig. 8). The importance of stratigraphy in shaping vertical walls is evident in the retrogressive process of the canyon flanks. This results in the exposure of vertical walls where rocky scarps of Miocene pre-canyon strata crop out. Two erosional processes influencing the retreatment of these vertical walls have been identified in the high-resolution bathymetries: ongoing mass-wasting and formation of gullies.

Mass-wasting processes predominantly occur through rock falls and spalling failures in most cases. Fallen blocks are chiefly observed at the base of cliffs and in association with terraces (Figs. 8D and 12D). Within the Blanes Canyon, it is common to observe the presence of small channels at the foot of the walls and terraces, referred to as moats. These little moats are presumably formed in response to bottom contour currents driven by persistent up- and down-canyon currents confined within the canyon. The development of these moats contributes significantly to wall undermining, leading to consequent destabilization due to loss of basal support. Besides, the loss of load during the wall retreat results in a release of internal stresses, leading to bedrock toppling. Similar occurrences have been reported in the Whittard Canyon (Carter et al., 2018).

The relationship between bedding and slope, observed at a broad-scale, is also evident at a finer scale. The mapped walls in the eastern flank tributary channel (Fig. 7) face the same direction as the dip of the strata (cataclinal slope), exhibiting further degradation attributed to the inclination of the weakness planes dipping in favor of the slope. This results in a highly irregular rim and preserved blocky slide deposits at the foot of the slope (Fig. 7A and D). Chaytor et al. (2016) related the partial absence of organisms attached to the walls as indicative of recent block falls. This theory could be applied in the case of a scar from a fallen block on the east flank wall of the channel (Fig. 13B), as it is surrounded by benthic fauna except for where the block should have been, proving that block falling is an ongoing process. Moreover, where the relief allows the fallen blocks to be sheltered from the axis currents, the preservation of these blocks is significantly higher, supporting active dynamics. The western flank of the tributary instead behaves as an orthoclinal to anaclinal slope, with continuous walls and a clean axis. The ongoing process of fine-scale mass wasting associated with the stratigraphy is comparable to the hypothesis of translational sliding on broad-scale cataclinal slopes presented in the previous section.

Spalling failure is another active process, as fresh evidence of this cliff retreat mechanism has been observed (Fig. 13C). Spalling failure associated with canyon walls is very common, regardless of the type of slope. Previous studies by McHugh et al. (1993), Chaytor et al. (2016) and Carter et al. (2018) have focused on the morphology and controls affecting this fracturing process associated with carbonate rockwalls. In the Blanes Canyon, the spalling failure occurs in Miocene sediment
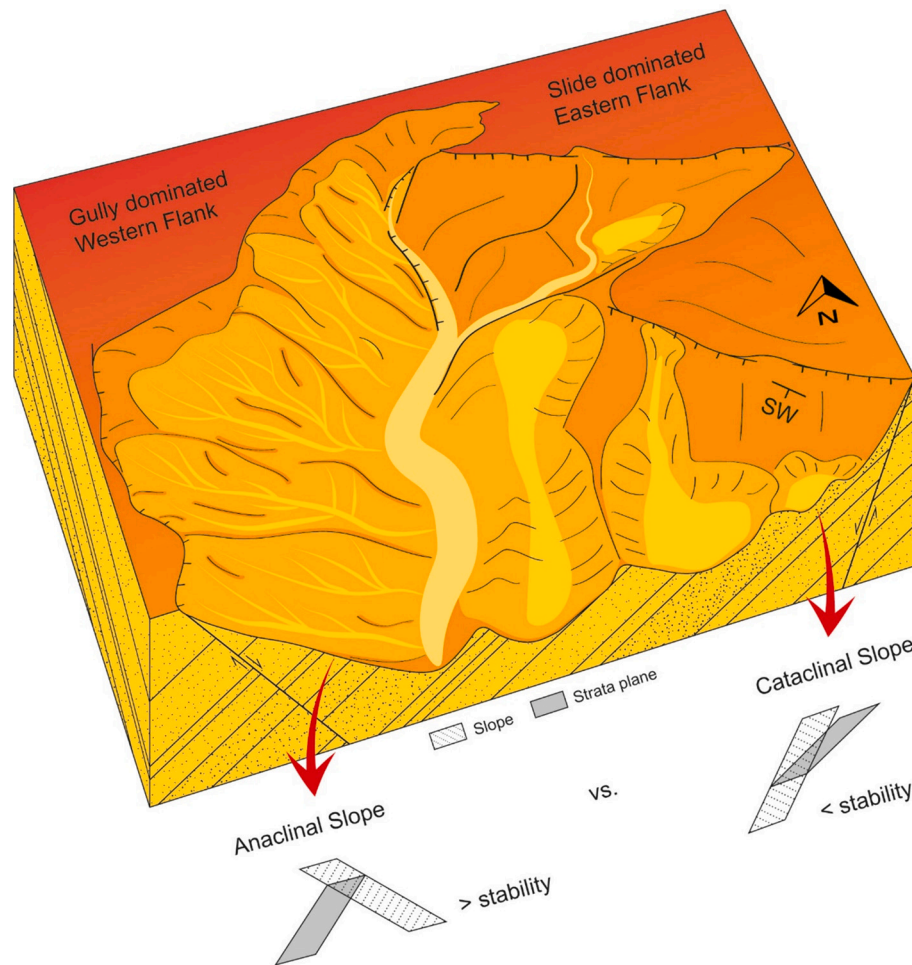
Fig. 14. Schematic representation of the interaction between the underneath stratigraphy and the relief of the Blanes Canyon, showing two types of slope, anaclinal slope (left) and cataclinal slope (right) and their effect on the resulting processes, a gully dominated western flank and a slide dominated eastern flank.

(ITGE, 1989), with an increased occurrence in relation to terraced areas and walls where moats appear. The process of spalling failure is related to the dilatation of diagenetic fractures caused by load loss and abrasion from sediment-laden contour currents (Mitchell, 2014). While the triggering mechanism for block fall and spalling failure is quite similar, the difference lies in whether the current acts on the walls in an abrasive manner, leading to spalling failure, or excavating the base, resulting in block fall.

The formation of gullies has been observed at different scales on vertical walls since the high gradient of these environments is necessary for gully development. Considering that the size of the gullies determines their maturity (García-García et al., 2012), different stages of their evolution have been observed: rills, emerging gullies and small gullies at fine-scale; and toe and rim gullies at broad-scale. The formation of rills corresponds to the earliest stage and reflects the sediment entrainment (Fig. 11C). Similar type of rills has been described in the Nazaré Canyon, but they were defined as fine-scale gullies (Masson et al., 2011). Here, we have differentiated rills from gullies based on their shallow penetration. The initiation of rills can occur either in relation to erosion by centimeter-scale rocks sliding or rolling downslope, or by excavation by small debris flows or turbidity currents (Masson et al., 2011). Within the Blanes Canyon, a real-time example of a small rock sliding down the slope during ROV dives was observed (see supplementary information, Video 1), suggesting this process as the potential origin of these morphologic features. A small slope retrogression aligned with rill lineations was also observed (Fig. 11C), providing evidence that these rills play a role in the initiation of the gullies. In the

geomorphological maps, the term "emerging gully" is used to describe a gully that has a penetration enough to maintain their position over time, ≤1 m deep (Figs. 8D, 9D and 10D). As the rills evolve, they become emerging gullies, representing the subsequent stage while maintaining their linearity. The last stage identified at fine-scale is the small gully stage (Figs. 8D and 12D). This stage marks the maturation of the emerging gullies through incision over a few meters and short upward erosion extending tens of meters. Meandering may even occur at this stage (Fig. 8D). The first two stages are only visible at a fine-scale, while the third stage is challenging to observed on a broad-scale. Toe gullies and rim gullies represent the final stages and are visible at canyon-scale reaching kilometer-long lengths (Fig. 3A and D), with dendritic rim gullies being the most mature of the classification.

Detailed examination of different morphologic features at fine-scale, including small moats bordering the base of walls and terraces, fresh scars due to mass wasting or the formation of rills, has revealed that despite the apparent inactivity of the canyon on a broad-scale, there is evident activity on a fine-scale. Additional fine-scale morphologic features further indicate active dynamics, such as evidenced by the presence of small furrows and ripples in the thalweg of the canyon (Fig. 9A and B). The presence of a green leaf of *Posidonia oceanica* over the ripples (Fig. 9B) not only provides insights into the direction of the current, but also confirms the active dynamics. The occurrence of this phanerogama is typically limited to depths ranging from 0 to 40 m on the continental shelf (Hartog and Kuo, 2006). Notably, the image captured at a depth of 650 m displays the *Posidonia oceanica* leaf in a fresh state, revealing a recent and ongoing process. Sanchez-Vidal et al. (2012) noted that

during strong storm conditions, such as the one occurred on 26th of December 2008 in the Blanes Canyon, coarse material from the shelf can be remobilized, reaching the canyon head and being funneled down-canyon, thus supporting this interpretation. In addition to this fine-scale activity, a recurrent pattern of processes is observed in the Blanes Canyon, where both fine- and broad-scale mass-wasting and gully formation processes dominate, conditioned in both cases by the type of slope. Exploring the fine-scale processes affecting vertical walls provides valuable insights into the short-term evolution of canyon flanks, particularly in the current context of highstand sea level, where canyon-scale activity is assumed to be reduced.

5.4. Human impact

Several morphologic features highlight the anthropogenic impact on the Blanes Canyon. On a broader scale, it has been observed that a large part of the western canyon rim is smoothed over the slope break (Fig. 3A and D). These smoother areas coincide with known fishing grounds, suggesting that the western rim may have been smoothed by recurrent trawling erosion, as proposed by Puig et al. (2012) in La Fonera Canyon, or that fishermen may be using the gentle relief of the rim for the establishment of their fishing grounds. On a finer scale, however, detailed examination through high-resolution bathymetry and ROV images have revealed trawl marks coinciding with trawler passage data even in areas of greater complexity, crossing the canyon thalweg (Figs. 10D and 11D). This observation suggests that fishermen do not always seek simple or easily accessible grounds when trawling, which raises the question: Was the rim previously smoothed or has it been eroded over decades of trawling activity?

6. Conclusions

The Blanes Canyon has been developed following a predetermined underlying tectonic structure and the influence of marine erosion-deposition since its formation in the Messinian.

The detailed examination of the broad-scale of the Blanes Canyon has provided valuable insights into the stratigraphical influence on the morphology and evolution of submarine canyons. The Blanes Canyon shows two asymmetrical flanks, whose evolution is controlled by the type of slope, which is determined by the stratigraphy. The eastern flank has a cataclinal slope and is dominated by translational slides and toe gullies in the most incised areas. In contrast, the western flank exhibits an orthoclinal to anaclinal slope and it is mainly dominated by rim gullies that increase in size with the increasing height of the flank.

High-resolution mapping of the canyon flanks using ROVs has enabled a detailed examination of vertical rockwalls that can be up to tens or even hundreds of meters high. The vertical walls exhibit a wide variety of fine-scale morphologic features and associated erosive processes, contributing to the wall retrogression and providing substrate for attached benthic communities.

As on a broader scale, the vertical walls are influenced by tectonics and regional stratigraphy, mainly located in areas where fault systems are emplaced and their retrogression is in favorable stratigraphy.

The primary mechanisms driving the retrogression of vertical walls are ongoing mass-wasting and gully formation. The main forms of mass-wasting are block-falling and spalling failure, both having a direct interaction with the fine-scale contour currents. The evolution of the gully formation process has been observed from its earliest stage (millimeter-scale rills) to the mature stage (kilometer-scale rim gullies), with a high gradient accompanied by a tractive force crucial to trigger them.

Understanding the processes shaping the fine-scale morphology of the submarine canyon is essential because it allows us to better understand the broad-scale morphology and their evolution over time. Additionally, it provides valuable information on the current activity of the canyon, which might not be discernible on a broad-scale. Moreover, the broad-scale morphology allows to contextualize the processes and morphologic features observed at fine-scale. A multi-scale study is therefore essential to better understand the spatio-temporal relationships of the underwater landscape throughout the geological record.

Supplementary data to this article can be found online at https://doi.org/10.1016/j.geomorph.2024.109290.

CRediT authorship contribution statement

C. Cabrera: Writing – review & editing, Writing – original draft, Visualization, Validation, Software, Resources, Methodology, Investigation, Formal analysis, Data curation, Conceptualization. **P. Puig:** Writing – review & editing, Writing – original draft, Visualization, Validation, Supervision, Resources, Project administration, Investigation, Funding acquisition, Formal analysis, Conceptualization. **R. Durán:** Writing – review & editing, Writing – original draft, Visualization, Validation, Supervision, Software, Resources, Methodology, Investigation, Formal analysis, Data curation, Conceptualization. **M.-C. Fabri:** Writing – review & editing, Validation, Resources, Methodology, Investigation, Formal analysis. **C. Guerin:** Writing – review & editing, Software, Resources, Methodology, Investigation, Formal analysis, Data curation. **C. Lo Iacono:** Writing – review & editing, Validation, Resources, Investigation, Formal analysis. **V.A.I. Huvenne:** Writing – review & editing, Validation, Resources, Investigation.

Declaration of competing interest

The authors declare that they have no known competing financial interests or personal relationships that could have appeared to influence the work reported in this paper.

Data availability

Data used in this study include bathymetric data from Secretariat General of the Fisheries (SGP) and TRAGSA. New data generated in this study can be provided upon reasonable request.

Acknowledgements

References

Allin, J.R., Hunt, J.E., Clare, M.A., Talling, P.J., 2018. Eustatic sea-level controls on the flushing of a shelf-incising submarine canyon. Geol. Soc. Am. Bull. 130, 222–237. https://doi.org/10.1130/B31658.1.

Amblas, D., Canals, M., Lastras, G., Berné, S., Loubrieu, B., 2004. Imaging the Seascapes. Oceanography 17, 144.

Amblas, D., Canals, M., Urgeles, R., Lastras, G., Liquete, C., Hughes-Clarke, J.E., Casamor, J.L., Calafat, A.M., 2006. Morphogenetic mesoscale analysis of the northeastern Iberian margin, NW Mediterranean Basin. Mar. Geol. 234, 3–20. https://doi.org/10.1016/j.margeo.2006.09.009.

Baztan, J., Berné, S., Olivet, J.L., Rabineau, M., Aslanian, D., Gaudin, M., Réhault, J.P., Canals, M., 2005. Axial incision: the key to understand submarine canyon evolution (in the western Gulf of Lion). Mar. Petrol. Geol. 22, 805–826. https://doi.org/10.1016/j.marpetgeo.2005.03.011.

Bernhardt, A., Melnick, D., Jara-Muñoz, J., Argandoña, B., González, J., Strecker, M.R., 2015. Controls on submarine canyon activity during sea-level highstands: the Biobío canyon system offshore Chile. Geosphere 11, 1226–1255. https://doi.org/10.1130/GES01063.1.

Bührig, L.H., Colombera, L., Patacci, M., Mountney, N.P., McCaffrey, W.D., 2022. Tectonic Influence on the Geomorphology of Submarine Canyons: Implications for Deep-Water Sedimentary Systems. Front. Earth Sci. 10, 836823 https://doi.org/10.3389/feart.2022.836823.

Canals, M., Casamor, J.L., Lastras, G., Monaco, A., Acosta, J., Berné, S., Loubrieu, B., Weaber, P.P.E., Greham, A., Dennielou, B., 2004. The Role of Canyons in Strata Formation. Oceanography 17, 80–91.

Canals, M., Company, J.B., Martín, D., Sanchez-Vidal, A., Ramirez-Llodra, E., 2013. Integrated study of Mediterranean deep canyons: Novel results and future challenges. Prog. Oceanogr. 118, 1–27. https://doi.org/10.1016/j.pocean.2013.09.004.

Carter, G.D., Huvenne, V.A., Gales, J.A., Iacono, C.L., Marsh, L., Ougier-Simonin, A., Robert, K., Wynn, R.B., 2018. Ongoing evolution of submarine canyon rockwalls; examples from the Whittard Canyon, Celtic margin (NE Atlantic). Prog. Oceanogr. 169, 79–88. https://doi.org/10.1016/j.pocean.2018.02.001.

Cerrillo-Escoriza, J., Lobo, F.J., Puga-Bernabéu, Á., Bárcenas, P., Mendes, I., Pérez-Asensio, J.N., Durán, R., Andersen, T.J., Carrión-Torrente, Á., García, M., López-Quirós, A., Luján, M., Mena, A., Sánchez-Guillamón, O., Sánchez, M.J., 2024. Variable downcanyon morphology controlling the recent activity of shelf-incised submarine canyons (Alboran Sea, western Mediterranean). Geomorphology 453, 109127. https://doi.org/10.1016/j.geomorph.2024.109127.

Chaytor, J.D., Demopoulos, A.W., ten Brink, U.S., Baxter, C., Quattrini, A.M., Brothers, D. S., 2016. Assessment of canyon wall failure process from multibeam bathymetry and Remotely Operated Vehicle (ROV) observations, US Atlantic continental margin. In: Lamarche, G., Mountjoy, J., Hubble, T., Krastel, S., Lane, E., Micallef, A., Moscardelli, L., Mueller, C., Pecher, I., Woelz, S. (Eds.), Submarine Mass Movements and their Consequences: 7th International Symposium. Springer International Publishing, pp. 103–113.

Clavell, E., Berastegui, X., 1991. Petroleum geology of the Gulf of Valencia. Generation, accumulation and production of Europe's hydrocarbons 7, 355–368.

Collier, J.S., Brown, C.J., 2005. Correlation of sidescan backscatter with grain size distribution of surficial seabed sediments. Mar. Geol. 214, 431–449. https://doi.org/10.1016/j.margeo.2004.11.011.

Covault, J.A., Kostic, S., Paull, C.K., Ryan, H.F., Fildani, A., 2014. Submarine channel initiation, filling and maintenance from sea-floor geomorphology and morphodynamic modelling of cyclic steps. Sedimentology 61, 1031–1054. https://doi.org/10.1111/sed.12084.

Davie, M.K., Buffett, B.A., 2003. Sources of methane for marine gas hydrate: inferences from a comparison of observations and numerical models. Earth Planet. Sci. Lett. 206, 51–63. https://doi.org/10.1016/S0012-821X(02)01064-6.

Dowdeswell, J.A., Cofaigh, C.Ó., Noormets, R., Larter, R.D., Hillenbrand, C.D., Benetti, S., Evans, J., Pudsey, C.J., 2008. A major trough-mouth fan on the continental margin of the Bellingshausen Sea, West Antarctica: the Belgica Fan. Mar. Geol. 252, 129–140. https://doi.org/10.1016/j.margeo.2008.03.017.

Durán, R., Canals, M., Lastras, G., Micallef, A., Amblas, D., Pedrosa-Pàmies, R., Sanz, J.L., 2013. Sediment dynamics and post-glacial evolution of the continental shelf around the Blanes submarine canyon head (NW Mediterranean). Prog. in Oceanogr. 118, 28–46. https://doi.org/10.1016/j.pocean.2013.07.031.

Durán, R., Canals, M., Sanz, J.L., Lastra, G., Amblas, D., Micallef, A., 2014. Morphology and sediment dynamics of the northern Catalan continental shelf, northwestern Mediterranean Sea. Geomorphology 204, 1–20. https://doi.org/10.1016/j.geomorph.2012.10.004.

Emery, K.O., 1980. Continental margins—classification and petroleum prospects. AAPG Bull. 64, 297–315. https://doi.org/10.1306/2F918973-16CE-11D7-8645000102C1865D.

Fabri, M.C., Dugornay, O., de La Bernardie, X., Guerin, C., Sanchez, P., Arnaubec, A., Autin, T., Piasco, R., Puig, P., 2022. 3D-representations for studying deep-sea coral habitats in the Lacaze-Duthiers Canyon, from geological settings to individual specimens. Deep-Sea Res. I Oceanogr. Res. Pap. 187, 103831 https://doi.org/10.1016/j.dsr.2022.103831.

Fedele, J.J., García, M.H., 2009. Laboratory experiments on the formation of subaqueous depositional gullies by turbidity currents. Mar. Geol. 258, 48–59. https://doi.org/10.1016/j.margeo.2008.11.004.

Fernandez-Arcaya, U., Ramirez-Llodra, E., Aguzzi, J., Allcock, A.L., Davies, J.S., Dissanayake, A., Harris, P., Howell, K., Huvenne, V.A.I., Macmillan-Lawler, M., Martín, J., Menot, L., Nizinski, M., Puig, P., Rowden, A.A., Sanchez, F., Van den Beld, I.M., 2017. Ecological role of submarine canyons and need for canyon conservation: a review. Front. Mar. Sci. 4, 5. https://doi.org/10.3389/fmars.2017.00005.

Fisher, W.L., Galloway, W.E., Steel, R.J., Olariu, C., Kerans, C., Mohrigh, D., 2021. Deep-water depositional systems supplied by shelf-incising submarine canyons: Recognition and significance in the geologic record. Earth Sci. Rev. 214, 103531 https://doi.org/10.1016/j.earscirev.2021.103531.

Forwick, M., Baeten, N.J., Vorren, T.O., 2009. Pockmarks in Spitsbergen fjords. Nor. J. Geol. 89, 65–77.

Gaida, T.C., Snellen, M., van Dijk, T.A., Simons, D.G., 2019. Geostatistical modelling of multibeam backscatter for full-coverage seabed sediment maps. Hydrobiologia 845, 55–79. https://doi.org/10.1007/s10750-018-3751-4.

García-García, A., Schoolmeester, T., Orange, D., Calafat, A., Fabres, J., Grossman, E., Field, M., Lorenson, T.D., Levey, M., Sansoucy, M., 2012. Recent sedimentary processes in the Cap de Creus canyon head and adjacent continental shelf, NE Spain:

evidence from multibeam bathymetry, sub-bottom profiles and coring. Int. Assoc. Sedimentol. Spec. Publ. 44, 71–98. https://doi.org/10.1002/9781118311172.ch4.

Gerber, T.P., Amblas, D., Wolinsky, M.A., Pratson, L.F., Canals, M., 2009. A model for the long-profile shape of submarine canyons. Case Rep. Med. 114, F3. https://doi.org/10.1029/2008JF001190.

Goff, J.A., Austin Jr., J.A., Gulick, S., Nordfjord, S., Christensen, B., Sommerfield, C., Olson, H., Alexander, C., 2005. Recent and modern marine erosion on the New Jersey outer shelf. Mar. Geol. 216, 275–296. https://doi.org/10.1016/j.margeo.2005.02.015.

Grelle, G., Revellino, P., Donnarumma, A., Guadagno, F.M., 2011. Bedding control on landslides: a methodological approach for computer-aided mapping analysis. Nat. Hazards Earth Syst. Sci. 11, 1395–1409. https://doi.org/10.5194/nhess-11-1395-2011.

Harris, P.T., Whiteway, T., 2011. Global distribution of large submarine canyons: Geomorphic differences between active and passive continental margins. Mar. Geol. 285, 69–86. https://doi.org/10.1016/j.margeo.2011.05.008.

Hartog, C., Kuo, J., 2006. 2006. Taxonomy and biogeography of seagrasses. In: Larkum, A.W., Orth, R.J., Duarte, C.M., Hartog, C.D., Kuo, J. (Eds.), Seagrasses: Biology, Ecology and Conservation. Springer, pp. 1–23.

He, Y., Xie, X., Kneller, B.C., Wang, Z., Li, X., 2013. Architecture and controlling factors of canyon fills on the shelf margin in the Qiongdongnan Basin, northern South China Sea. Mar. Pet. Geol. 41, 264–276. https://doi.org/10.1016/j.marpetgeo.2012.03.002.

Huvenne, V.A., Tyler, P.A., Masson, D.G., Fisher, E.H., Hauton, C., Hühnerbach, V., Le Bas, T.P., Wolff, G.A., 2011. A picture on the wall: innovative mapping reveals cold-water coral refuge in submarine canyon. PloS One 6, e28755. https://doi.org/10.1371/journal.pone.0028755.

IGC-ICC, 2010. Atles geologic de Catalunya. Institut Geològic de Catalunya, Barcelona, Spain, 463pp.

ITGE, 1989. Mapa Geológico de la Plataforma Continental Española y Zonas Adyacentes 1:200 000. Hoja 35/42E (Barcelona). Instituto Tecnológico GeoMinero de España, Madrid, Spain, p. 10.

Kenyon, N.H., 1987. Mass-wasting features on the continental slope of Northwest Europe. Mar. Geol. 74, 57–77. https://doi.org/10.1016/0025-3227(87)90005-3.

Laberg, J.S., Guidard, S., Mienert, J., Vorren, T.O., Haflidason, H., Nygård, A., 2007. Morphology and morphogenesis of a high-latitude canyon; the Andøya Canyon, Norwegian Sea. Mar. Geol. 246, 68–85. https://doi.org/10.1016/j.margeo.2007.01.009.

Lastras, G., Arzola, R.G., Masson, D.G., Wynn, R.B., Huvenne, V.A.I., Hühnerbach, V., Canals, M., 2009. Geomorphology and sedimentary features in the Central Portuguese submarine canyons, Western Iberian margin. Geomorphology 103, 310–329. https://doi.org/10.1016/j.geomorph.2008.06.013.

Lastras, G., Canals, M., Amblas, D., Lavoie, C., Church, I., De Mol, B., Durán, R., Calafat, A.M., Hughes-Clarke, J.E., Smith, C.J., Heussner, S., 2011. Understanding sediment dynamics of two large submarine valleys from seafloor data: Blanes and La Fonera canyons, northwestern Mediterranean Sea. Mar. Geol. 280, 20–39. https://doi.org/10.1016/j.margeo.2010.11.005.

Li, W., Li, S., Alves, T.M., Rebesco, M., Feng, Y., 2021. The role of sediment gravity flows on the morphological development of a large submarine canyon (Taiwan Canyon), north-east South China Sea. Sedimentology 68, 1091–1108. https://doi.org/10.1111/sed.12818.

Lo, C.M., Weng, M.C., 2017. Identification of deformation and failure characteristics in cataclinal slopes using physical modeling. Landslides 14, 499–515.

Maillard, A., Mauffret, A., 1999. Crustal structure and riftogenesis of the Valencia Trough (North-Western Mediterranean Sea). Basin Res. 11, 357–379. https://doi.org/10.1046/j.1365-2117.1999.00105.x.

Maillard, A., Mauffret, A., Watts, A.B., Torné, M., Pascal, G., Buhl, P., Pinet, B., 1992. Tertiary sedimentary histori and structure of the Valencia Trough (western Mediterranean). Tectonophysics 203, 57–75. https://doi.org/10.1016/0040-1951(92)90215-R.

Maillard, A., Gorini, C., Mauffret, A., Sage, F., Lofi, J., Gaullier, V., 2006. Offshore evidence of polyphase erosion in the Valencia Basin (Northwestern Mediterranean): scenario for the Messinian Salinity Crisis. Sediment. Geol. 188-189, 69–91. https://doi.org/10.1016/j.sedgeo.2006.02.006.

Masson, D.G., Huvenne, V.A.I., de Stigter, H.C., Arzola, R.G., LeBas, T.P., 2011. Sedimentary processes in the middle Nazaré Canyon. Deep-Sea Res. II Top. Stud. Oceanogr. 58, 2369–2387. https://doi.org/10.1016/j.dsr2.2011.04.003.

McHugh, C.M., Ryan, W.B., Schreiber, B.C., 1993. The role of diagenesis in exfoliation of submarine canyons. AAPG Bull. 77, 145–172. https://doi.org/10.1306/BDFF8BB4-1718-11D7-8645000102C1865D.

Mercier, L., Migeon, S., Dall'Asta, M., Praeg, D., Rubino, J.L., Delhaye-Prat, V., Lafont, F., Akpi, T., 2023. Rectangular drainage pattern of a submarine canyon controlled by extensional tectonic structures: Case study of the Afam Incision Surface (Tortonian, Niger Delta, Nigeria). Mar. Geol. 462, 107093 https://doi.org/10.1016/j.margeo.2023.107093.

Micallef, A., Mountjoy, J.J., 2011. A topographic signature of a hydrodynamic origin for submarine gullies. Geology 39, 115–118. https://doi.org/10.1130/G31475.1.

Micallef, A., Mountjoy, J.J., Canals, M., Lastras, G., 2012. Deep-seated bedrock landslides and submarine canyon evolution in an active tectonic margin: Cook Strait, New Zealand. In: Yamada, Y., Kawamura, K., Ikehara, K., Ogawa, Y., Urgeles, R., Mosher, D., Chaytor, J., Strasser, M. (Eds.), Submarine Mass Movements and their Consequences: 5th International Symposium. Springer International Publishing, pp. 201–212.

Mitchell, N.C., 2006. Morphologies of knickpoints in submarine canyons. Geol. Soc. Am. Bull. 118, 589–605. https://doi.org/10.1130/B25772.1.

Mitchell, N.C., 2014. Bedrock erosion by sedimentary flows in submarine canyons. Geosphere 10, 892–904. https://doi.org/10.1130/GES01008.1.

Mountjoy, J.J., Barnes, P.M., Pettinga, J.R., 2009. Morphostructure and evolution of submarine canyons across an active margin: Cook Strait sector of the Hikurangi margin, New Zealand. Mar. Geol. 260, 45–68. https://doi.org/10.1016/j.margeo.2009.01.006.

Nakajima, T., Kakuwa, Y., Yasudomi, Y., Itaki, T., Motoyama, I., Tomiyama, T., Machiyama, H., Katayama, H., Okitsu, O., Morita, S., Tanahasi, M., Matsumoto, R., 2014. Formation of pockmarks and submarine canyons associated with dissociation of gas hydrates on the Joetsu Knoll, eastern margin of the Sea of Japan. J. Asian Earth Sci. 90, 228–242. https://doi.org/10.1016/j.jseaes.2013.10.011.

Naranjo-Vesga, J., Paniagua-Arroyave, J.F., Ortiz-Karpf, A., Jobe, Z., Wood, L., Galindo, P., Shumaker, L., Mateus-Tarazona, D., 2022. Controls on submarine canyon morphology along a convergent tectonic margin. The Southern Caribbean of Colombia. Mar. Petrol. Geol. 137, 105493 https://doi.org/10.1016/j.marpetgeo.2021.105493.

Normark, W.R., Piper, D.J.W., 1991. Initiation processes and flow evolution of turbidity currents: Implications for the depositional record. In: Osborne, R.H. (Ed.), From Shoreline to Abyss, SEPM, Spec. Pub, vol. 46, pp. 207–230.

Orejas, C., Gori, A., Iacono, C.L., Puig, P., Gili, J.M., Dale, M.R., 2009. Cold-water corals in the Cap de Creus canyon, northwestern Mediterranean: spatial distribution, density and anthropogenic impact. Mar. Ecol. Prog. Ser. 397, 37–51. https://doi.org/10.3354/meps08314.

Palanques, A., Puig, P., Latasa, M., Scharek, R., 2009. Deep sediment transport induced by storms and dense shelf-water cascading in the northwestern Mediterranean basin. Deep-Sea Res. I Oceanogr. Res. Pap. 56, 425–434. https://doi.org/10.1016/j.dsr.2008.11.002.

Palma, F.I., Bozzano, G., Principi, S., Isola, J.I., Ormazabal, J.P., Esteban, F.D., Tassone, A.A., 2021. Geomorphology and sedimentary processes on the Sloggett Canyon, Northwestern Scotia Sea. Argentina. J. S. Am. Earth Sci. 107, 103136 https://doi.org/10.1016/j.jsames.2020.103136.

Paradis, S., Puig, P., Masqué, P., Juan-Díaz, X., Martín, J., Palanques, A., 2017. Bottom-trawling along submarine canyons impacts deep sedimentary regimes. Sci. Rep. 7, 1–12 doi:10.1038%2Fsrep43332.

Paull, C.K., Ussler III, W., Mitts, P.J., Caress, D.W., West, G.J., 2006. Discordant 14C-stratigraphies in upper Monterey Canyon: a signal of anthropogenic disturbance. Mar. Geol. 233, 21–36. https://doi.org/10.1016/j.margeo.2006.07.008.

Paull, C.K., Caress, D.W., Lundsten, E., Gwiazda, R., Anderson, K., McGann, M., Conrad, J., Edwards, B., Sumner, E.J., 2013. Anatomy of the La Jolla submarine canyon system; offshore Southern California. Mar. Geol. 335, 16–34. https://doi.org/10.1016/j.margeo.2012.10.003.

Pearman, T.R., Robert, K., Callaway, A., Hall, R.A., Mienis, F., Huvenne, V.A., 2023. Spatial and temporal environmental heterogeneity induced by internal tides influences faunal patterns on vertical walls within a submarine canyon. Front. Mar. Sci. 10, 1091855. https://doi.org/10.3389/fmars.2023.1091855.

Poncelet, C., Billant, G., Corre, M.P, 2020. Globe (GLobal Oceanographic Bathymetry Explorer) Software. https://doi.org/10.17882/70460.

Pratson, L.F., Coakley, B.J., 1996. A model for the headward erosion of submarine canyons induced by downslope-eroding sediment flows. Geol. Soc. Am. Bull. 108, 225–234. https://doi.org/10.1130/0016-7606(1996)108%3C0225:AMFTHE%3E2.3.CO;2.

Puig, P., Canals, M., Company, J.B., Martín, J., Amblas, D., Lastras, G., Palanques, A., Calafat, A.M., 2012. Ploughing the deep sea floor. Nature 489, 286–289. https://doi.org/10.1038/nature11410.

Puig, P., Palanques, A., Martín, J., 2014. Contemporary sediment-transport processes in submarine canyons. Ann. Rev. Mar. Sci. 6, 53–77. https://doi.org/10.1146/annurev-marine-010213-135037.

Rahiman, T.I., Pettinga, J.R., 2006. The offshore morpho-structure and tsunami sources of the Viti Levu Seismic Zone, Southeast Viti Levu. Fiji. Mar. Geol. 232, 203–225. https://doi.org/10.1016/j.margeo.2006.07.007.

Restrepo-Correa, I.C., Ojeda, G.Y., 2010. Geologic controls on the morphology of La Aguja submarine canyon. J. South Am. Earth Sci. 29, 861–870. https://doi.org/10.1016/j.jsames.2010.07.001.

Riboulot, V., Cattaneo, A., Sultan, N., Garziglia, S., Ker, S., Imbert, P., Voisset, M., 2013. Sea-level change and free gas occurrence influencing a submarine landslide and

pockmark formation and distribution in deepwater Nigeria. Earth Planet. Sc. Lett. 375, 78–91. https://doi.org/10.1016/j.epsl.2013.05.013.

Riboulot, V., Imbert, P., Cattaneo, A., Voisset, M., 2019. Fluid escape features as relevant players in the enhancement of seafloor stability? Terra Nova 31, 540–548. https://doi.org/10.1111/ter.12425.

Riera, R., Paumard, V., de Gail, M., Saqab, M.M., Lebrec, U., Lang, S.C., Lane, A., 2022. Origin of seafloor pockmarks overlying submarine landslides: Insights from semi-automated mapping of 3D seismic horizons (North West Shelf, Australia). Mar. Pet. Geol. 136, 105453 https://doi.org/10.1016/j.marpetgeo.2021.105453.

Robert, K., Huvenne, V.A., Georgiopoulou, A., Jones, D.O., Marsh, L., Carter, D.O., Chaumillon, L., 2017. New approaches to high-resolution mapping of marine vertical structures. Sci. Rep. 7, 9005. https://doi.org/10.1038/s41598-017-09382-z.

Roca, E., Sans, M., Cabrera, L., Marzo, M., 1999. Oligocene to Middle Miocene evolution of the central Catalan margin (northwestern Mediterranean). Tectonophysic 315, 209–233. https://doi.org/10.1016/S0040-1951(99)00289-9.

Sanchez-Vidal, A., Canals, M., Calafat, A.M., Lastras, G., Pedrosa-Pàmies, R., Menéndez, M., Medina, R., Company, J.B., Hereu, B., Romero, J., Alcoverro, T., 2012. Impacts on the deep-sea ecosystem by a severe coastal storm. PloS One 7, e30395. https://doi.org/10.1371/journal.pone.0030395.

Scarselli, N., 2020. Submarine landslides–architecture, controlling factors and environments. A summary. In: Scarselli, N., Adam, J., Chiarella, D. (Eds.), Regional Geology and Tectonics: Volume 1: Principles of Geologic Analysis, 2nd Edition ed. Elsevier, pp. 417–439. https://doi.org/10.1016/B978-0-444-64134-2.00015-8.

Serra Raventós, J., 1975. El precontinente catalán entre Cap Begur y Arenys de Mar (Provs. de Gerona y Barcelona): estructura y sedimentación reciente. In: PhD Thesis, 187 pp.

Shepard, F.P., 1981. Submarine canyons: multiple causes and long-time persistence. AAPG Bull. 65, 1062–1077. https://doi.org/10.1306/03B59459-16D1-11D7-8645000102C1865D.

Soutter, E.L., Kane, I.A., Hodgson, D.M., Flint, S., 2021. The concavity of submarine canyon longitudinal profiles. J. Geophys. Res-earth. 126, e2021JF006185 https://doi.org/10.1029/2021JF006185.

Sultan, N., Cochonat, P., Canals, M., Cattaneo, A., Dennielou, B., Haflidason, H., Laberg, J.S., Long, D., Mienert, J., Trincardi, F., Urgeles, R., Vorren, T.O., Wilson, C., 2004. Triggering mechanisms of slope instability processes and sediment failures on continental margins: a geotechnical approach. Mar. Geol. 213, 291–321. https://doi.org/10.1016/j.margeo.2004.10.011.

Tassone, A., Roca, E., Muñoz, J.A., Cabrera, L., Canals, M., 1994. Evolución del sector septentrional del margen continental catalán durante el Cenozoico. Acta Geológica Hispánica 29, 3–37.

Tubau, X., Lastras, G., Canals, M., Micallef, A., Amblas, D., 2013. Significance of the fine drainage pattern for submarine canyon evolution: the Foix Canyon System, Northwestern Mediterranean Sea. Geomorphology 184, 20–37. https://doi.org/10.1016/j.geomorph.2012.11.007.

Uchupi, E., Emery, K.O., 1991. Genetic global geomorphology: A prospectus. In: Osborne, R.H. (Ed.), From Shoreline to Abyss: Contributions in Marine Geology in Honor of Francis Parker Shepard. SEPM Special Publication, Tulsa, Oklahoma, pp. 273–290.

Varnes, D.J., 1978. Slope movement types and processes. In: Schuster, R.L., Krizek, R. J (Eds.), Landslides: analysis and control. Transportation Research Board, National Research Council, Washington, DC, pp. 12–33.

Wan, L., Hurter, S., Bianchi, V., Li, P., Wang, J., Salles, T., 2022. The roles and seismic expressions of turbidites and mass transport deposit using stratigraphic forward modeling and seismic forward modeling. J. Asian Earth Sci. 232, 105110 https://doi.org/10.1016/j.jseaes.2022.105110.

Zhu, M., Graham, S., Pang, X., McHargue, T., 2010. Characteristics of migrating submarine canyons from the middle Miocene to present: Implications for paleoceanographic circulation, northern South China Sea. Mar. Petrol. Geol. 27, 307–319. https://doi.org/10.1016/j.marpetgeo.2009.05.005.

Zúñiga, D., Flexas, M.M., Sanchez-Vidal, A., Coenjaerts, J., Calafat, A., Jordà, G., García-Orellana, J., Puigdefàbregas, J., Canals, M., Espino, M., Sardà, F., Company, J.B., 2009. Particle fluxes dynamics in Blanes submarine canyon (Northwestern Mediterranean). Prog. Oceanogr. 82, 239–251. https://doi.org/10.1016/j.pocean.2009.07.002.